fluids

MDPI

Article

Navier–Stokes Equations and Bulk Viscosity for a Polyatomic Gas with Temperature-Dependent Specific Heats

Shingo Kosuge [1] and Kazuo Aoki [2,*]

[1] Institute for Liberal Arts and Sciences, Kyoto University, Kyoto 606-8501, Japan; kosuge.shingo.6r@kyoto-u.ac.jp
[2] Department of Mathematics, National Cheng Kung University, Tainan 70101, Taiwan
* Correspondence: kazuo.aoki.22v@st.kyoto-u.ac.jp

Abstract: A system of Navier–Stokes-type equations with two temperatures is derived, for a polyatomic gas with temperature-dependent specific heats (thermally perfect gas), from the ellipsoidal statistical (ES) model of the Boltzmann equation extended to such a gas. Subsequently, the system is applied to the problem of shock-wave structure for a gas with large bulk viscosity (or, equivalently, with slow relaxation of the internal modes), and the numerical results are compared with those based on the ordinary Navier–Stokes equations. It is shown that the latter equations fail to describe the double-layer structure of shock profiles for a gas with large bulk viscosity.

Keywords: polyatomic gases; bulk viscosity; Navier–Stokes equations; ES model; shock-wave structure; thermally perfect gases

Citation: Kosuge, S.; Aoki, K. Navier–Stokes Equations and Bulk Viscosity for a Polyatomic Gas with Temperature-Dependent Specific Heats. *Fluids* **2023**, *8*, 5. https://doi.org/10.3390/fluids8010005

Academic Editors: Elena Kustova and Rakesh Kumar

Received: 11 November 2022
Revised: 10 December 2022
Accepted: 16 December 2022
Published: 22 December 2022

1. Introduction

Nonequilibrium flows of polyatomic gases have attracted increasing attention in connection with practical problems in high-temperature gas dynamics [1–4]. The basis of the study of such flows is kinetic theory of gases based on the Boltzmann Equation [3,5–8]. However, since the Boltzmann equation has a complicated structure particularly for polyatomic gases, simplified Boltzmann equations for a polyatomic gas, in which the internal states are represented by a single variable associated with the energy of internal modes, have been proposed [9–14]. It should be mentioned that recent progress in the mathematical study of these Boltzmann equations is remarkable [12,14–17].

However, even the simplified versions of the Boltzmann equation are still not simple enough for practical applications. Therefore, alternative approaches using model Boltzmann equations [18–27] or macroscopic equations [28–35] have been proposed. The model Boltzmann equations bear much simpler structures while retaining certain basic properties of the original Boltzmann equation. The ellipsoidal-statistical (ES) model [21,22] is one of such models and is relevant herein. The macroscopic equations partially take account of kinetic effects of polyatomic gases, such as bulk viscosity, empirically or systematically on the basis of kinetic theory.

In a recent paper by the present authors, M. Bisi, and M. Groppi [36], a set of Navier–Stokes-type equations with two temperatures [two-temperature Navier–Stokes (NS) equations for short] was derived on the basis of kinetic theory and applied successfully to the structure of a plane shock wave for a polyatomic gas with large bulk viscosity. More specifically, the set was derived by the Chapman–Enskog procedure [37–40] using the ES model under the assumption that the relaxation of the internal modes is slow. It should be noted that, in this model, this assumption corresponds to large bulk viscosity.

The two-temperature NS equations in [36] are for a gas with constant specific heats (calorically perfect gas), since they were derived using the ES model for such a gas. In reality, however, the specific heats for most gases are temperature-dependent even when treated conceptually as ideal gases (thermally perfect gas). The effect of temperature-dependent

specific heats becomes particularly important when there are significant variations in temperature in the flow field, such as gas flows containing strong shock waves.

For this reason, herein, we attempt to extend the two-temperature NS equations to a gas with temperature-dependent specific heats. Since the ES model has been extended to such a gas in [41], we will adopt this extended ES model as the starting point. Subsequently, an analysis can be conducted in parallel to [36], and given that the analysis details have already been published, we simply provide the result herein. We then shift our attention to a comparison between the ordinary Navier–Stokes (NS) equations with a single temperature, in which the bulk viscosity is contained, and the two-temperature NS equations, in which the bulk viscosity does not occur. The comparison is performed numerically for the structure of a plane shock wave.

Here, the following comments are in order. Navier–Stokes-type equations with two or multiple temperatures have widely been used in computational fluid dynamics for hypersonic flows of real gases in connection with reentry flight and contributed to the development of aerothermodynamics [2,3,42,43]. These flows comprise mixtures of many component gases with dissociation and chemical reactions. Because of the complexity of the phenomena, the equations are not strictly based on kinetic theory, and various modelings are introduced in many different processes. In this sense, the approach is different from ours that originates from kinetic theory in a simpler and idealized setting. Moreover, it is worth mentioning that the relation between multi-temperature fluid models and the bulk viscosity has been discussed on the basis of kinetic theory [44,45].

The rest of the paper is organized as follows. We summarize the extended ES model for a gas with temperature-dependent specific heats and its basic properties in Section 2. Next, the ordinary NS equations with a single temperature and the two-temperature NS equations, both derived from the extended ES model, are summarized in Sections 3 and 4, respectively. Brief remarks on the relation between the bulk viscosity and the presence of the two temperatures, the translational and internal temperatures, are given in Section 5. In Section 6, the shock-structure problem is analyzed numerically for certain gases with large bulk viscosities using the two different NS equations, and the difference in the shock profiles is discussed. Section 7 provides concluding remarks.

2. ES Model for a Gas with Temperature-Dependent Specific Heats

Let us consider a polyatomic rarefied gas. Let t be the time variable, $\boldsymbol{X}$ (or X_i) the position vector in the physical space, $\boldsymbol{\xi}$ (or ξ_i) the molecular velocity, and $\mathcal{E}$ the energy associated with the internal modes per unit mass. We denote by

$$f(t, \boldsymbol{X}, \boldsymbol{\xi}, \mathcal{E}) d\boldsymbol{X} d\boldsymbol{\xi} d\mathcal{E}, \tag{1}$$

the total mass of the gas molecules contained in an infinitesimal volume $d\boldsymbol{X}d\boldsymbol{\xi}d\mathcal{E}$ around a point $(\boldsymbol{X}, \boldsymbol{\xi}, \mathcal{E})$ in the seven-dimensional space consisting of $\boldsymbol{X}$, $\boldsymbol{\xi}$, and $\mathcal{E}$ at time t. We may call $f(t, \boldsymbol{X}, \boldsymbol{\xi}, \mathcal{E})$ the velocity–energy distribution function of the gas molecules.

2.1. ES Model

In the present paper, the gas is assumed to be thermally perfect, that is, the specific heat at constant volume c_{v} and that at constant pressure c_{p} are not constant but are functions of the temperature T. For such a gas, an ES model governing the velocity-energy distribution function f was proposed in [41]. It is a straightforward extension of the ES model for a gas with constant c_{v} and c_{p} [21]. In this subsection, we summarize the ES model proposed in [41].

We first consider an equilibrium state with a uniform and constant temperature T and assume for the moment that the specific heats are independent of T and that the classical equipartition law holds. Then, the internal energy E of the gas per unit mass can be expressed as $E = (3 + \delta_0)RT/2$, where δ_0 is the (constant) number of internal degrees of freedom, and R is the gas constant per unit mass (note that $R = k_{\mathrm{B}}/m$ with k_{B} the Boltzmann constant and m the mass of a gas molecule). Now, we consider a more general

gas for which the internal energy E is a given (monotonically increasing) function of the temperature T, i.e., $E = E(T)$. Then, we define a function $D(T)$ as $D(T) = 2E(T)/RT - 3$. This $D(T)$ is a *generalized* number of internal degrees of freedom. Note that the relations $c_{\mathrm{v}}(T) = dE(T)/dT$ and $c_{\mathrm{p}}(T) = c_{\mathrm{v}}(T) + R$ hold, so that c_{v} and c_{p} depend on the temperature.

Next, we apply the functions $E(T)$, $D(T)$, $c_{\mathrm{v}}(T)$, and $c_{\mathrm{p}}(T)$, defined in the equilibrium, to the nonequilibrium situation and use them in the construction of the ES model for the thermally perfect gas. We omit the process of the construction (see [41]) and simply show the result. The ES model is given by the following equation:

$$\frac{\partial f}{\partial t} + \xi_i \frac{\partial f}{\partial X_i} = Q(f), \tag{2}$$

where

$$Q(f) = A_c(T)\rho(\mathcal{G} - f). \tag{3}$$

Here,

$$\mathcal{G} = \frac{\rho \mathcal{E}^{\delta/2-1}}{(2\pi)^{3/2}[\det(\mathsf{T})]^{1/2}(RT_{\mathrm{rel}})^{\delta/2}\Gamma(\delta/2)} \times \exp\left(-\frac{1}{2}(\mathsf{T}^{-1})_{ij}(\xi_i - v_i)(\xi_j - v_j) - \frac{\mathcal{E}}{RT_{\mathrm{rel}}}\right), \tag{4a}$$

$$(\mathsf{T})_{ij} = (1-\theta)[(1-\nu)RT_{\mathrm{tr}}\delta_{ij} + \nu p_{ij}/\rho] + \theta RT\delta_{ij}, \tag{4b}$$

$$\rho = \iint_0^\infty f d\mathcal{E} d\boldsymbol{\xi}, \qquad v_i = \frac{1}{\rho}\iint_0^\infty \xi_i f d\mathcal{E} d\boldsymbol{\xi}, \tag{4c}$$

$$p_{ij} = \iint_0^\infty (\xi_i - v_i)(\xi_j - v_j) f d\mathcal{E} d\boldsymbol{\xi}, \tag{4d}$$

$$T = E^{-1}(e), \qquad \delta = D(T) = 2E(T)/RT - 3 = 2e/RT - 3, \tag{4e}$$

$$T_{\mathrm{tr}} = 2e_{\mathrm{tr}}/3R, \qquad T_{\mathrm{int}} = 2e_{\mathrm{int}}/R\delta, \qquad T_{\mathrm{rel}} = \theta T + (1-\theta)T_{\mathrm{int}}, \tag{4f}$$

where e, e_{tr}, and e_{int} are defined by

$$e = e_{\mathrm{tr}} + e_{\mathrm{int}}, \quad e_{\mathrm{tr}} = \frac{1}{2\rho}\iint_0^\infty |\boldsymbol{\xi} - \boldsymbol{v}|^2 f d\mathcal{E} d\boldsymbol{\xi}, \quad e_{\mathrm{int}} = \frac{1}{\rho}\iint_0^\infty \mathcal{E} f d\mathcal{E} d\boldsymbol{\xi}. \tag{5}$$

In (2)–(5), ρ is the density, $\boldsymbol{v}$ (or v_i) is the flow velocity, p_{ij} is the stress tensor, e is the internal energy per unit mass, e_{tr} is that associated with the translational motion, e_{int} is that associated with the internal modes, T is the temperature, T_{tr} is the temperature associated with the translational motion, T_{int} is the temperature associated with the energy of the internal modes, $d\boldsymbol{\xi} = d\xi_1 d\xi_2 d\xi_3$, and the domain of integration with respect to $\boldsymbol{\xi}$ is the whole space of $\boldsymbol{\xi}$. The symbol δ_{ij} indicates the Kronecker delta, and $\nu \in [-1/2, 1)$ and $\theta \in [0, 1]$ are parameters. In addition, $A_c(T)$ is a function of T such that $A_c(T)\rho$ is the collision frequency of the gas molecules, $\Gamma(z) = \int_0^\infty s^{z-1}e^{-s}ds$ is the gamma function, T is the 3×3 positive-definite symmetric matrix whose (i, j) component is defined by (4b), and $\det(\mathsf{T})$ and T^{-1} are, respectively, its determinant and inverse.

Note that all the macroscopic quantities contained in $\mathcal{G}$ are generated from f. To be more specific, (i) ρ, $\boldsymbol{v}$, p_{ij}, e_{tr}, e_{int}, and e are obtained by (4c), (4d) and (5); (ii) T and then δ are determined by (4e) using the inverse function E^{-1} of the function E; (iii) T_{tr}, T_{int}, and T_{rel} are determined by (4f), and then T is established by (4b). Since $e = e_{\mathrm{tr}} + e_{\mathrm{int}} = (3T_{\mathrm{tr}} + \delta T_{\mathrm{int}})R/2$ and also $e = (3+\delta)RT/2$, we have the relation $T = (3T_{\mathrm{tr}} + \delta T_{\mathrm{int}})/(3+\delta)$ [note that δ depends on T: cf. (4e)].

The pressure p and the heat-flow vector q_i are given by

$$p = R\rho T, \tag{6a}$$

$$q_i = \iint_0^\infty (\xi_i - v_i)\left(\frac{1}{2}|\boldsymbol{\xi} - \boldsymbol{v}|^2 + \mathcal{E}\right) f d\mathcal{E} d\boldsymbol{\xi}, \tag{6b}$$

where (6a) is the equation of state.

2.2. Basic Properties

In this subsection, we summarize the basic properties that follow from the model Equation (2) [41]. Some properties are different when the parameter θ is equal to zero.

- *Conservations*: For an arbitrary function $f(t, \boldsymbol{X}, \boldsymbol{\xi}, \mathcal{E})$, the following relation holds:

$$\iint_0^\infty \varphi_r Q(f) d\mathcal{E} d\boldsymbol{\xi} = 0, \tag{7}$$

  where φ_r ($r = 0, \ldots, 4$) are $\varphi_0 = 1$, $\varphi_i = \xi_i$ ($i = 1, 2, 3$), and $\varphi_4 = \frac{1}{2}|\boldsymbol{\xi}|^2 + \mathcal{E}$ for $\theta \neq 0$; and φ_r ($r = 0, \ldots, 5$) are $\varphi_0 = 1$, $\varphi_i = \xi_i$ ($i = 1, 2, 3$), $\varphi_4 = \frac{1}{2}|\boldsymbol{\xi}|^2$, and $\varphi_5 = \mathcal{E}$ for $\theta = 0$.

- *Equilibrium*: The vanishing of the collision term $Q(f) = 0$ is equivalent to the fact that f is the following local equilibrium distribution:

$$f_{\mathrm{eq}} = \frac{\bar{\rho}\mathcal{E}^{\bar{\delta}/2-1}}{(2\pi R\bar{T})^{3/2}(R\bar{T})^{\bar{\delta}/2}\Gamma(\bar{\delta}/2)} \exp\left(-\frac{|\boldsymbol{\xi} - \bar{\boldsymbol{v}}|^2}{2R\bar{T}} - \frac{\mathcal{E}}{R\bar{T}}\right), \tag{8}$$

  for $\theta \neq 0$, where $\bar{\rho}$, $\bar{\boldsymbol{v}}$, and $\bar{T}$ are arbitrary functions of t and $\boldsymbol{X}$, and $\bar{\delta} = D(\bar{T})$; and

$$f_{\mathrm{eq}} = \frac{\bar{\rho}\mathcal{E}^{\bar{\delta}/2-1}}{(2\pi R\bar{T}_{\mathrm{tr}})^{3/2}(R\bar{T}_{\mathrm{int}})^{\bar{\delta}/2}\Gamma(\bar{\delta}/2)} \exp\left(-\frac{|\boldsymbol{\xi} - \bar{\boldsymbol{v}}|^2}{2R\bar{T}_{\mathrm{tr}}} - \frac{\mathcal{E}}{R\bar{T}_{\mathrm{int}}}\right), \tag{9}$$

  for $\theta = 0$, where $\bar{\rho}$, $\bar{\boldsymbol{v}}$, $\bar{T}_{\mathrm{tr}}$, and $\bar{T}_{\mathrm{int}}$ are arbitrary functions of t and $\boldsymbol{X}$, and $\bar{\delta}$ and $\bar{T}$ are determined by the following coupled equations:

$$\bar{\delta} = D(\bar{T}), \qquad \bar{T} = E^{-1}(3R\bar{T}_{\mathrm{tr}}/2 + \bar{\delta}R\bar{T}_{\mathrm{int}}/2). \tag{10}$$

  The solution $(\bar{\delta}, \bar{T})$ of (10) exists. In particular, it is unique when $\bar{T}_{\mathrm{int}} \leq \bar{T}_{\mathrm{tr}}$.

- *Entropy inequality: For an arbitrary function $f(t, \boldsymbol{X}, \boldsymbol{\xi}, \mathcal{E})$, the following inequality holds:*

$$\iint_0^\infty \left(\ln \frac{f}{\mathcal{E}^{\delta/2-1}}\right) Q(f) d\mathcal{E} d\boldsymbol{\xi} \leq 0, \tag{11}$$

  where δ is defined by (4e) and (5). The equality sign holds if and only if $f = f_{\mathrm{eq}}$ in (8) ($\theta \neq 0$) or (9) ($\theta = 0$).

- *Mean free path*: The mean free path l_0 of the gas molecules in the equilibrium state at rest, at density ρ_0, and temperature T_0 is given by

$$l_0 = \frac{2}{\sqrt{\pi}} \frac{(2RT_0)^{1/2}}{A_c(T_0)\rho_0}, \tag{12}$$

  for the ES model (2), since $A_c(T_0)\rho_0$ is the collision frequency at this equilibrium state.

- *Relaxation*: In the space homogeneous case, where $f = f(t, \boldsymbol{\xi}, \mathcal{E})$, the macroscopic quantities ρ, $\boldsymbol{v}$, and T are constant, and the temperatures T_{tr} and T_{int} relax to T in the following manner:

$$T_{\mathrm{tr}} = T + (T_{\mathrm{tr}*} - T)\, e^{-\theta A_c(T)\rho t}, \tag{13a}$$

$$T_{\mathrm{int}} = T + (T_{\mathrm{int}*} - T)\, e^{-\theta A_c(T)\rho t}. \tag{13b}$$

  where $T_{\mathrm{tr}*}$ and $T_{\mathrm{int}*}$ are, respectively, the values of T_{tr} and T_{int} at the initial time $t = 0$ satisfying the relation $(3T_{\mathrm{tr}*} + \delta T_{\mathrm{int}*})/(3+\delta) = T$ with $\delta = D(T)$. Since $1/A_c(T)\rho$ is the mean free time, the time scale of relaxation of the temperatures is the mean free time devided by θ. Therefore, we may regard θ as the parameter controlling the speed of relaxation of the internal modes. This situation is the same as in the case of the ES model with constant δ [36].

It should be remarked that the inequality (11) enables us to show the H-theorem only for the spatially homogeneous case [41]. It is a drawback of this model, which should be the consequence of the simple and convenient definition of the temperature T and the resulting δ using the given function E [cf. (4e)].

3. Ordinary Navier–Stokes Equations with a Single Temperature

When the mean free path l_0 of the gas molecules in the reference equilibrium state at rest with density ρ_0 and temperature T_0 is much shorter than the characteristic length L of the system, i.e., when the Knudsen number $\mathrm{Kn} = l_0/L$ is small, one can formally derive fluid-dynamic equations by a classical procedure, such as the Chapman–Enskog expansion, from the ES model (2). In this section, restricting ourselves to the case where θ is of the order of unity, we summarize the Navier–Stokes equations derived in [41] by the standard Chapman–Enskog procedure.

The macroscopic quantities ρ, v_i, and T are governed by the following Navier–Stokes equations for a compressible fluid:

$$\frac{\partial \rho}{\partial t} + \frac{\partial \rho v_j}{\partial X_j} = 0, \tag{14a}$$

$$\frac{\partial \rho v_i}{\partial t} + \frac{\partial \rho v_i v_j}{\partial X_j} = -\frac{\partial p}{\partial X_i} + \frac{\partial}{\partial X_j}\left[\mu(T)\left(\frac{\partial v_i}{\partial X_j} + \frac{\partial v_j}{\partial X_i} - \frac{2}{3}\frac{\partial v_k}{\partial X_k}\delta_{ij}\right)\right] + \frac{\partial}{\partial X_i}\left[\mu_b(T)\frac{\partial v_k}{\partial X_k}\right], \tag{14b}$$

$$\frac{\partial}{\partial t}\left[\rho\left(\frac{3+\delta}{2}RT + \frac{1}{2}|\boldsymbol{v}|^2\right)\right] + \frac{\partial}{\partial X_j}\left[\rho v_j\left(\frac{5+\delta}{2}RT + \frac{1}{2}|\boldsymbol{v}|^2\right)\right] = \frac{\partial}{\partial X_j}\left[\lambda(T)\frac{\partial T}{\partial X_j}\right] + \frac{\partial}{\partial X_j}\left[\mu(T)v_i\left(\frac{\partial v_i}{\partial X_j} + \frac{\partial v_j}{\partial X_i} - \frac{2}{3}\frac{\partial v_k}{\partial X_k}\delta_{ij}\right)\right] + \frac{\partial}{\partial X_j}\left[\mu_b(T)v_j\frac{\partial v_k}{\partial X_k}\right], \tag{14c}$$

with $p = R\rho T$ [cf. (6a)] and $\delta = D(T)$. Here, the viscosity $\mu(T)$, the bulk viscosity $\mu_b(T)$, and the thermal conductivity $\lambda(T)$ are given by

$$\mu(T) = \mathrm{Pr}\frac{RT}{A_c(T)}, \qquad \mu_b(T) = \frac{1}{\theta}\left[\frac{5}{3} - \gamma(T)\right]\frac{1}{\mathrm{Pr}}\mu(T),$$
$$\lambda(T) = \frac{\gamma(T)}{\gamma(T)-1}R\frac{RT}{A_c(T)}, \qquad \mathrm{Pr} = \frac{1}{1-\nu+\theta\nu}, \tag{15}$$

where $\gamma(T) = c_{\rm p}(T)/c_{\rm v}(T) = [c_{\rm v}(T) + R]/c_{\rm v}(T)$ is the ratio of the specific heats, and ${\rm Pr} = c_{\rm p}(T)\mu(T)/\lambda(T)$ is the Prandtl number. In addition, the translational and internal temperatures $T_{\rm tr}$ and $T_{\rm int}$ are, respectively, given as

$$T_{\rm tr} = T - \frac{1}{R}\mu_b(T)\frac{1}{\rho}\frac{\partial v_k}{\partial X_k}, \qquad T_{\rm int} = T + \frac{3}{R\delta}\mu_b(T)\frac{1}{\rho}\frac{\partial v_k}{\partial X_k}. \tag{16}$$

One of the advantages of the present ES model is that the resulting transport coefficients (15) are simple and explicit, so that the Navier–Stokes Eqaution (14) have a wide applicability for practical flows of a polyatomic gas with temperature-dependent specific heats.

4. Navier–Stokes Equations with Two Temperatures

In this section, we consider the case where the parameter θ contained in the ES model (2) is small. As was seen in Section 2.2, this corresponds to the case with slow relaxation of the internal modes. On the other hand, Equation (15) indicates that small values of θ correspond to large values of the ratio μ_b/μ of the bulk viscosity to the viscosity.

In [36], the case where θ is small and of the same order of magnitude as the Knudsen number Kn ($\ll 1$) was considered for the ES model for a gas with constant specific heats, and fluid-dynamic equations were derived by an adapted Chapman–Enskog expansion. The fluid-dynamic equations are of Navier–Stokes type containing two temperatures, the temperature associated with the energy of the internal modes and that associated with the translational energy, and relaxation terms of the temperatures.

If we let

$$\theta = \alpha\epsilon, \qquad \epsilon = (\sqrt{\pi}/2){\rm Kn} \ll 1, \tag{17}$$

where α is a positive constant of the order of unity, in the ES model (2) and carry out almost the same analysis using the Chapman–Enskog expansion for small ϵ as in [36], we obtain the equations of Navier–Stokes type with two temperatures. In this paper, the process of analysis is omitted, and only the result is shown. The dimensional form of the resulting equations is as follows:

$$\frac{\partial \rho}{\partial t} + \frac{\partial \rho v_j}{\partial X_j} = 0, \tag{18a}$$

$$\frac{\partial \rho v_i}{\partial t} + \frac{\partial \rho v_i v_j}{\partial X_j} = -\frac{\partial \rho R T_{\rm tr}}{\partial X_i} + \frac{\partial}{\partial X_j}\left[\mu(T, T_{\rm tr})\left(\frac{\partial v_i}{\partial X_j} + \frac{\partial v_j}{\partial X_i} - \frac{2}{3}\frac{\partial v_k}{\partial X_k}\delta_{ij}\right)\right], \tag{18b}$$

$$\begin{aligned}&\frac{\partial}{\partial t}\left[\rho\left(\frac{3}{2}RT_{\rm tr} + \frac{1}{2}|\boldsymbol{v}|^2\right)\right] + \frac{\partial}{\partial X_j}\left[\rho v_j\left(\frac{5}{2}RT_{\rm tr} + \frac{1}{2}|\boldsymbol{v}|^2\right)\right] + \theta A_c(T)\rho^2 \cdot \frac{3}{2}R(T_{\rm tr} - T)\\ &\quad = \frac{\partial}{\partial X_j}\left[\lambda(T, T_{\rm tr})\frac{\partial T_{\rm tr}}{\partial X_j}\right] + \frac{\partial}{\partial X_j}\left[\mu(T, T_{\rm tr})v_i\left(\frac{\partial v_i}{\partial X_j} + \frac{\partial v_j}{\partial X_i} - \frac{2}{3}\frac{\partial v_k}{\partial X_k}\delta_{ij}\right)\right],\end{aligned} \tag{18c}$$

$$\begin{aligned}&\frac{\partial}{\partial t}\left(\rho\frac{\delta}{2}RT_{\rm int}\right) + \frac{\partial}{\partial X_j}\left(\rho v_j\frac{\delta}{2}RT_{\rm int}\right) + \theta A_c(T)\rho^2 \cdot \frac{\delta}{2}R(T_{\rm int} - T)\\ &\quad = \frac{1}{5}\frac{\partial}{\partial X_j}\left[\lambda(T, T_{\rm tr})\frac{\partial \delta T_{\rm int}}{\partial X_j}\right],\end{aligned} \tag{18d}$$

with

$$T = \frac{3T_{\rm tr} + \delta T_{\rm int}}{3 + \delta}, \qquad \delta = D(T), \tag{19}$$

where the viscosity $\mu(T,\, T_{\rm tr})$ and the thermal conductivity $\lambda(T,\, T_{\rm tr})$ are given, respectively, by

$$\mu(T,\, T_{\rm tr}) = \frac{1}{1-\nu}\frac{RT_{\rm tr}}{A_c(T)}, \qquad \lambda(T,\, T_{\rm tr}) = \frac{5}{2}R\frac{RT_{\rm tr}}{A_c(T)}. \tag{20}$$

With the known functions $A_c(T)$ and $D(T)$, the system (18)–(20) form the equations for ρ, v_i, T, $T_{\rm tr}$, and $T_{\rm int}$. It is shown in Appendix A in [41] that a solution $(T,\, \delta)$ of (19) exists for given $T_{\rm tr}$ and $T_{\rm int}$ under the assumption that $E(T) > 3RT/2$. When $T_{\rm int} < T_{\rm tr}$, T is such that $T_{\rm int} < T < T_{\rm tr}$, and the solution $(T,\, \delta)$ is unique; when $T_{\rm tr} < T_{\rm int}$, T is such that $T_{\rm tr} < T < T_{\rm int}$, and the possibility that the solution is not unique is not excluded depending on the form of $E(T)$ (see Appendix A in [41]). If the solution is not unique, it is not clear if there is a criterion to choose one of the solutions. In the numerical examples of shock-wave structure in Section 6.3, $T_{\rm int} < T_{\rm tr}$ holds in all cases. Finally, it should be recalled that θ in (18) is small as indicated by (17).

5. Some Remarks

The ordinary NS Equation (14) are based on the Navier–Stokes constitutive relations, i.e., the following expressions of the stress tensor p_{ij} and the heat-flow vector q_i:

$$p_{ij} = p\delta_{ij} - \mu(T)\left(\frac{\partial v_i}{\partial X_j} + \frac{\partial v_j}{\partial X_i} - \frac{2}{3}\frac{\partial v_k}{\partial X_k}\delta_{ij}\right) - \mu_b(T)\frac{\partial v_k}{\partial X_k}\delta_{ij}, \tag{21a}$$

$$q_i = -\lambda(T)\frac{\partial T}{\partial X_i}. \tag{21b}$$

Here, we should recall that Equation (21) has been derived under the assumption that θ is of the order of unity. On the other hand, the viscosity μ and the bulk viscosity μ_b make sense only for the stress tensor p_{ij} of the form of (21a). Suppose that we are able to measure, experimentally, the tangential and normal stresses as well as the flow velocity, pressure, and temperature. Then, the viscosity and the bulk viscosity are determined empirically with the help of (21a). It is known that there are many gases that have large values of the ratio μ_b/μ. However, it follows from (15) that large μ_b/μ means small θ. Therefore, for the gases with large μ_b/μ, the appropriate fluid-dynamic equations are not (14), derived under the assumption $\theta = O(1)$, but (18), derived under (17). This fact was already pointed out in [36] for a gas with constant specific heats. In the next section, we will compare the shock-wave structure based on (18) and that based on (14) for some gases with large μ_b/μ numerically and find that they are significantly different.

The Chapman–Enskog expansion has been carried out for the dimensionless form of (2) in terms of the small parameter ϵ in (17). Equations (14) and (18) retain the terms of $O(1)$ and $O(\epsilon)$ though it is not visible from the dimensional Equations (14) and (18). It is noted that the terms containing $\mu(T)$, $\mu_b(T)$, and $\lambda(T)$ in (14) and those containing $\mu(T,\, T_{\rm tr})$, $\lambda(T,\, T_{\rm tr})$, and θ in (18) correspond to the terms of $O(\epsilon)$. Equation (14) with $p = R\rho T$ and $\delta = D(T)$ determines ρ, v, T, and p; then, Equation (16) gives $T_{\rm tr}$ and $T_{\rm int}$ as small perturbations of $O(\epsilon)$ from T. In this way, $T_{\rm tr}$ and $T_{\rm int}$ play a subsidiary role.

When μ_b/μ is large, as can be guessed from (16), $T_{\rm tr}$ and $T_{\rm int}$ are not small perturbations from T and play a principal role. Therefore, we need the principal equations governing $T_{\rm tr}$ and $T_{\rm int}$, which are given by the system (18). The transition from (18) to (14) for θ such that $O(\epsilon) \ll \theta \ll O(1)$ can be shown by following the procedure in [44], as in the case of a gas with constant specific heats (see Appendix B in [46]).

6. Shock-Wave Structure

The problem of shock-wave structure is one of the most fundamental problems in kinetic theory and has been investigated for long time [6,39,40,47]. In this section, we investigate the problem of shock-wave structure for some gases with large values of μ_b/μ using the two-temperature NS Equation (18) as well as the ordinary NS Equation (14) and compare the results.

A typical example of a polyatomic gas with large μ_b/μ is CO_2, and the study of shock-wave structure for CO_2 gas, which has a long history [48–51], has been revived in recent years [31,33,35,52–57]. For instance, an interesting classification of shock profiles depending on the upstream Mach number was provided in [52,53] using macroscopic equations based on extended thermodynamics. The results in [31,52,53] were subsequently confirmed by kinetic theory, more precisely, by the numerical analysis using the ES model in [41,58].

The first aim of this section is to confirm that the two-temperature NS equations (18) are able to reproduce the shock profiles obtained by the ES model (2) for a gas with temperature dependent specific heats [41]. The second aim is to assess the validity of the ordinary NS equations (14) with large bulk viscosity by comparing the obtained shock profiles with those based on the two-temperature NS equations (18).

6.1. Problem

We consider a stationary plane shock wave in a uni-directional flow of an ideal polyatomic gas with large values of μ_b/μ, i.e., with slow relaxation of the internal modes, perpendicular to the shock wave. The X_1 axis of the coordinate system is taken in the flow direction. The gas at upstream infinity ($X_1 \to -\infty$) is in an equilibrium state with density ρ_-, flow velocity $\boldsymbol{v}_- = (v_-, 0, 0)$, and temperature T_-, while the gas at downstream infinity ($X_1 \to +\infty$) is in another equilibrium state with density ρ_+, flow velocity $\boldsymbol{v}_+ = (v_+, 0, 0)$, and temperature T_+. We investigate the steady behavior of the gas under the following assumptions: (i) the specific heat at constant volume $c_{\rm v}$ is a known function of the temperature T; (ii) the behavior of the gas is described by the Navier–Stokes equations with a single temperature (14) or those with two temperatures (18); (iii) the problem is spatially one dimensional, so that the physical quantities are independent of X_2 and X_3.

Let us denote by M_- the Mach number at upstream infinity and by γ_- the ratio of the specific heats at the temperature T_-, i.e.,

$$M_- = \frac{v_-}{\sqrt{\gamma_- R T_-}}, \qquad \gamma_- \equiv \gamma(T_-) = \frac{c_{\rm v}(T_-) + R}{c_{\rm v}(T_-)}. \tag{22}$$

When $\theta \neq 0$, the downstream parameters ρ_+, v_+, T_+ and the upstream ones ρ_-, v_-, T_- are related by the following Rankine–Hugoniot relations [41]:

$$\frac{\rho_+}{\rho_-} = \left(\frac{v_+}{v_-}\right)^{-1}, \qquad \frac{v_+}{v_-} = \frac{1 + \gamma_- M_-^2 - \sqrt{2\gamma_- M_-^2 \hat{d}_E(\tau) + 1}}{\gamma_- M_-^2}, \qquad \frac{T_+}{T_-} = \tau, \tag{23}$$

where

$$\hat{d}_E(x) = \frac{1}{R}\int_1^x c_{\rm v}(T_- s) ds, \tag{24}$$

and τ is a solution such that $\tau > 1$ of the following equation:

$$\tau + 2\hat{d}_E(\tau) + \frac{1}{\gamma_- M_-^2} - \left(\frac{1}{\sqrt{\gamma_-} M_-} + \sqrt{\gamma_-} M_-\right)\sqrt{2\hat{d}_E(\tau) + \frac{1}{\gamma_- M_-^2}} = 0. \tag{25}$$

If $c_{\rm v}(T)$ is the increasing function of T, the solution satisfying $\tau > 1$ is unique [41].

We try to obtain the numerical solutions of the steady and one-dimensional versions of (14) and (18), where $\partial/\partial t = \partial/\partial X_2 = \partial/\partial X_3 = 0$ and $v_2 = v_3 = 0$ are assumed, under the following boundary conditions:

$$(\rho, v_1, T) \to (\rho_\mp, v_\mp, T_\mp), \quad \text{as} \quad X_1 \to \mp\infty, \quad [\text{for (14)}], \tag{26a}$$

$$(\rho, v_1, T_{\rm tr}, T_{\rm int}) \to (\rho_\mp, v_\mp, T_\mp, T_\mp), \quad \text{as} \quad X_1 \to \mp\infty, \quad [\text{for (18)}]. \tag{26b}$$

In the actual computation, however, we solve corresponding time-dependent problems and obtain the steady shock profiles as the long-time limit of the unsteady solutions. Since the numerical method is essentially the same as that in [36], we omit its description here.

6.2. Properties of Some Gases with Large Bulk Viscosities

In Table IV in [46], thermophysical properties of some gases with large ratios of the bulk viscosity to the viscosity are listed. In this paper, we choose SF_6, CH_4, and CO_2 from the list and investigate the shock-wave structure for these gases.

We first consider the specific heat at constant volume $c_v(T)$ according to the data of that at constant pressure $c_p(T)$ in [59,60]. We use the following fitting formula for $c_v(T)$:

$$c_v(T)/R = c_0 + c_1\,T + c_2\,T^2 + c_3\,T^3 + c_4\,T^4, \tag{27}$$

where $c_0, \ldots, c_4$ are fitting coefficients having units such that each term on the right-hand side is dimensionless. The values of $c_0, \ldots, c_4$ listed in Table 1 are those determined by using the data in [59,60] for SF_6 and CH_4 and those taken from [31] for CO_2. In the table, the values of $c_v(T_-)/R$, $\gamma_-\,[=\gamma(T_-)]$, and $\delta_- \equiv D(T_-)$ when $T_- = 300\,\mathrm{K}$ are also shown. Figure 1 shows the comparison between the fitting formula (27) with the values in Table 1 and the data in [59,60]. It is seen that the formula (27) reproduces the data well for the temperature range between 220 K and 1100 K. If $T_- = 300\,\mathrm{K}$ and $M_- = 5$, then $T_+ = 1.938T_- \approx 581\,\mathrm{K}$ for SF_6, $T_+ = 3.408T_- \approx 1022\,\mathrm{K}$ for CH_4, and $T_+ = 3.708T_- \approx 1112\,\mathrm{K}$ for CO_2.

Table 1. The coefficients in the fitting formula (27) and $c_v(T_-)$, γ_-, and δ_- for $T_- = 300\,\mathrm{K}$ for SF_6, CH_4, and CO_2.

	c_0	c_1	c_2	c_3	c_4	$c_v(T_-)/R$	γ_-	δ_-
SF_6	−4.017	7.670(−2) [a]	−1.130(−4)	7.745(−8)	−2.014(−11)	10.75	1.093	18.50
CH_4	3.505	−7.952(−3)	3.221(−5)	−2.829(−8)	8.280(−12)	3.322	1.301	3.643
CO_2	1.412 [b]	8.697(−3) [b]	−6.575(−6) [b]	1.987(−9) [b]	0	3.483	1.287	3.966

[a] Read as 7.670×10^{-2}; [b] Value in [31].

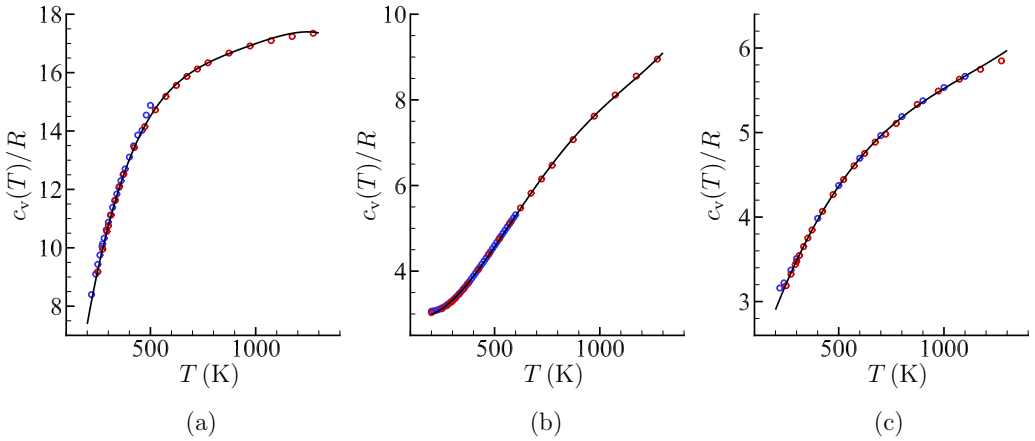

Figure 1. $c_v(T)/R$ vs. T. (**a**) SF_6, (**b**) CH_4, and (**c**) CO_2. The solid line indicates the fitting Formula (27) with the data in Table 1, the red circles represent the data from [60], and the blue circles denote those from [59].

Other thermophysical properties for SF_6, CH_4, and CO_2 are included in Table IV in [46]. The data for these three gases are shown in Table 2. The data for the viscosity μ, the ratio of the specific heats γ, and the Prandtl number Pr, which are at $T = 300\,\mathrm{K}$ and $p = 101\,\mathrm{kPa}$, are taken from [59], whereas those for the ratio μ_b/μ, which are at $T = 300\,\mathrm{K}$, are taken from [61]. Note that for the ES model, μ depends only on T. From these data, one obtains the values of θ and ν in Table 2 by using (15). As expected, the values of θ are small.

In [46], the viscosity $\mu(T)$ was assumed to be in the form

$$\mu(T) = \mu(300\,\mathrm{K}) \times (T/300\,\mathrm{K})^s, \tag{28}$$

and the exponent s was determined by using the method of least squares on the basis of the data provided in [59]. The obtained value of s for each gas is shown in Table 2. Equation (28) with these values of s reproduces the data of μ given in [62] quite well in the temperature range 250–1300 K for CO_2 and 250–600 K for SF_6 and CH_4. The function $A_c(T)$ is then determined by (15) as

$$A_c(T) = A_c(300\,\mathrm{K}) \times \left(\frac{T}{300\,\mathrm{K}}\right)^{1-s}, \quad A_c(300\,\mathrm{K}) = (R\mathrm{Pr}) \times \left[\frac{300\,\mathrm{K}}{\mu(300\,\mathrm{K})}\right]. \tag{29}$$

With this $A_c(T)$, the reference mean free path l_0 is obtained by (12).

Table 2. Thermophysical properties of some gases with large bulk viscosities.

	μ [10^{-6} Pa · s]	s	γ	Pr	μ_b/μ	$\theta \times 10^3$	ν
SF_6	15.24 [a]	0.90	1.097 [a]	0.806 [a]	320 [b]	2.21	−0.241
CH_4	11.43 [a]	0.83	1.305 [a]	0.7630 [a]	240 [b]	1.98	−0.311
CO_2	14.91 [a]	0.83	1.293 [a]	0.767 [a]	3849 [b]	0.127	−0.304

[a] Value at 300 K, 101 kPa in [59]; [b] Value at 300 K in [61].

6.3. Numerical Results

In this section, we show some numerical results for the three gases mentioned in Section 6.2, i.e., CO_2, SF_6, and CH_4. The shock-wave structure based on the two-temperature NS equations (18) is compared with that based on the ordinary NS equations (14). For CO_2 gas, it is also compared with the result based on the original ES model (2) taken from [41].

As in [41,58], we show the profiles of the density ρ, the flow velocity v_1 (the X_1 component), and the temperatures T, T_{tr}, and T_{int} normalized in the conventional way, i.e.,

$$\check{\rho} = \frac{\rho - \rho_-}{\rho_+ - \rho_-}, \quad \check{v} = \frac{v_1 - v_+}{v_- - v_+}, \quad \check{T} = \frac{T - T_-}{T_+ - T_-}, \quad \check{T}_{\mathrm{tr}} = \frac{T_{\mathrm{tr}} - T_-}{T_+ - T_-}, \quad \check{T}_{\mathrm{int}} = \frac{T_{\mathrm{int}} - T_-}{T_+ - T_-}. \tag{30}$$

In this normalization, $\check{\rho}$, $\check{T}$, $\check{T}_{\mathrm{tr}}$, and $\check{T}_{\mathrm{int}}$ varies from 0 (upstream infinity) to 1 (downstream infinity), whereas $\check{v}$ from 1 (upstream infinity) to 0 (downstream infinity). In the figures in this section, the X_1 coordinate is normalized by the mean free path l_- at the equilibrium state at rest with density ρ_- and temperature T_-, i.e., $l_- = (2/\sqrt{\pi})(2RT_-)^{1/2}/A_c(T_-)\rho_-$ [cf. (12)], and the origin $X_1 = 0$ is set in such a way that $\check{\rho}$ obtained by (18) and that by (14) coincide at $X_1 = 0$. Otherwise, the absolute location of the origin is unimportant in the present problem. Here, it is put around the position where the density exhibits the steepest change, so that we can use the grid points concentrating on the origin in the numerical analysis.

6.3.1. CO_2 Gas

First, it should be noted that the calculation for CO_2 gas is carried out for the parameters slightly different from those shown in Tables 1 and 2 because one of the purposes here is to compare the result with that based on the original ES model (2) reported in [41]. In [41], T_- and p_- are set to be $T_- = 295$ K and $p_- = 69$ mmHg, respectively, in accordance with [31,53], and this T_- gives $c_{\mathrm{v}}(T_-)/R = 3.456$, $\gamma_- = 1.289$, and $\delta_- = 3.913$. In addition, although the fitting formula (27) with the data in Table 1 is used for $c_{\mathrm{v}}(T)/R$, the exponent s in (28) and (29) and Pr are set as $s = 0.935$ and Pr $= 0.73$, respectively.

One of the interests in this study is to observe the change of the shock-wave structure as the ratio μ_b/μ increases. For this purpose, we do not fix the value of μ_b/μ according to the thermophysical data, such as 3849 in Table 2, but specify it arbitrary; we assume $\mu_b/\mu = 10$, 100, and 1000 in the following. In other words, our CO_2 gas is a fictitious

one that we called the *pseudo*-CO_2 gas in [58]. Correspondingly, the parameter θ becomes $\theta = 5.169 \times 10^{-2}$, 5.169×10^{-3}, and 5.169×10^{-4}, respectively.

Figures 2–4 show the profiles of $\check{\rho}$, $\check{v}$, $\check{T}$, $\check{T}_{\rm tr}$, and $\check{T}_{\rm int}$ inside the shock wave at $M_- = 1.3$ in the case of the pseudo-CO_2 gas; Figure 2 is for $\mu_b/\mu = 10$, Figure 3 for $\mu_b/\mu = 100$, and Figure 4 for $\mu_b/\mu = 1000$. Note that $T_+/T_- = 1.141$ and $\rho_+/\rho_- = (p_+/p_-)(T_-/T_+) = 1.566$ at $M_- = 1.3$. In each of Figures 2–4, panel (a) shows the profiles of $\check{\rho}$, $\check{v}$, and $\check{T}$, and panel (b) those of $\check{T}$, $\check{T}_{\rm tr}$, and $\check{T}_{\rm int}$; in Figure 4, panels (c) and (d) are, respectively, the magnified figures of panels (a) and (b). The solid line indicates the result based on the two-temperature NS equations (18), and the dot-dashed line that based on the ordinary NS equation (14). The respective macroscopic quantities are shown in different colors, which can be recognized from the colors of the labels on the vertical axis. To be more specific, the red, green, and blue lines indicate, respectively, $\check{\rho}$, $\check{v}$, and $\check{T}$ in panels (a) and (c) and $\check{T}_{\rm tr}$, $\check{T}_{\rm int}$, and $\check{T}$ in panels (b) and (d). In Figures 3 and 4, $\check{\rho}$, $\check{v}$, $\check{T}$, $\check{T}_{\rm tr}$, and $\check{T}_{\rm int}$ obtained by using the ES model (2) [41] is also shown by the black dashed line, and in Figure 4c,d, the result based on the ordinary NS equations is not included. In addition, in Figure 4, the result for $\theta = 0$ (or $\mu_b/\mu = \infty$), obtained by the two-temperature NS equations, is shown by dotted lines. It should be noted that the Rankine–Hugoniot relations are different from (23) when $\theta = 0$ (see Appendix B.2 in [41]).

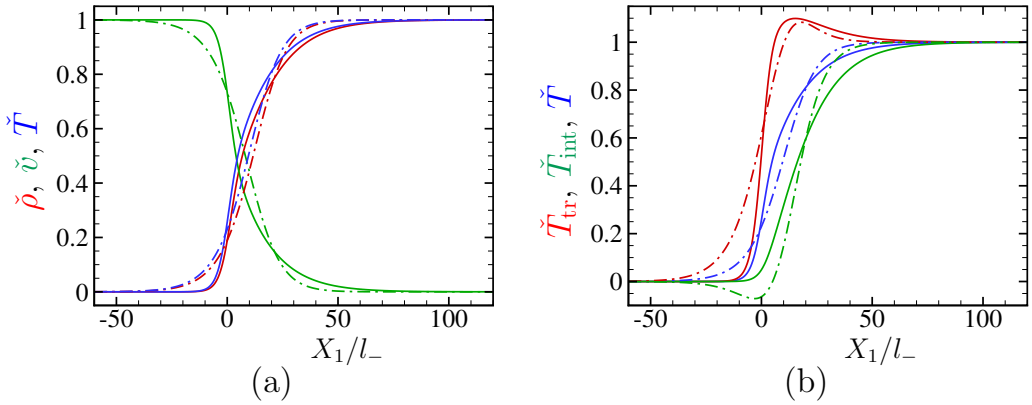

Figure 2. Profiles of $\check{\rho}$, $\check{v}$, $\check{T}$, $\check{T}_{\rm tr}$, and $\check{T}_{\rm int}$ in the case of the pseudo-CO_2 gas at $M_- = 1.3$ for $\mu_b/\mu = 10$. (**a**) $\check{\rho}$, $\check{v}$, and $\check{T}$; (**b**) $\check{T}_{\rm tr}$, $\check{T}_{\rm int}$, and $\check{T}$. The solid line indicates the result based on the two-temperature NS equations (18), and the dot-dashed line that based on the ordinary NS equations (14). The red, green, and blue lines indicate, respectively, $\check{\rho}$, $\check{v}$, and $\check{T}$ in panel (**a**) and $\check{T}_{\rm tr}$, $\check{T}_{\rm int}$, and $\check{T}$ in panel (**b**).

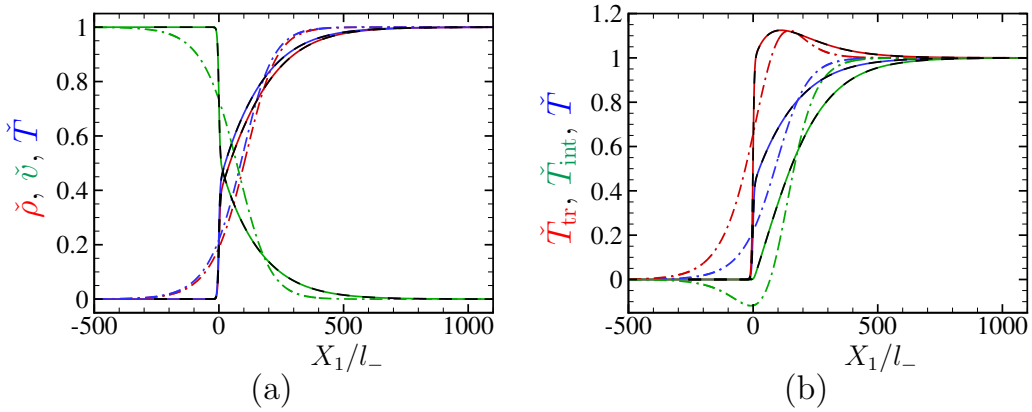

Figure 3. Profiles of $\check{\rho}$, $\check{v}$, $\check{T}$, $\check{T}_{\rm tr}$, and $\check{T}_{\rm int}$ in the case of the pseudo-CO_2 gas at $M_- = 1.3$ for $\mu_b/\mu = 100$. (**a**) $\check{\rho}$, $\check{v}$, and $\check{T}$; (**b**) $\check{T}_{\rm tr}$, $\check{T}_{\rm int}$, and $\check{T}$. The solid line indicates the result based on the two-temperature NS equations (18), and the dot-dashed line that based on the ordinary NS equations (14). The red, green, and blue lines indicate, respectively, $\check{\rho}$, $\check{v}$, and $\check{T}$ in panel (**a**) and $\check{T}_{\rm tr}$, $\check{T}_{\rm int}$, and $\check{T}$ in panel (**b**). The profiles based on the ES model (2) are shown by the black dashed line for all quantities.

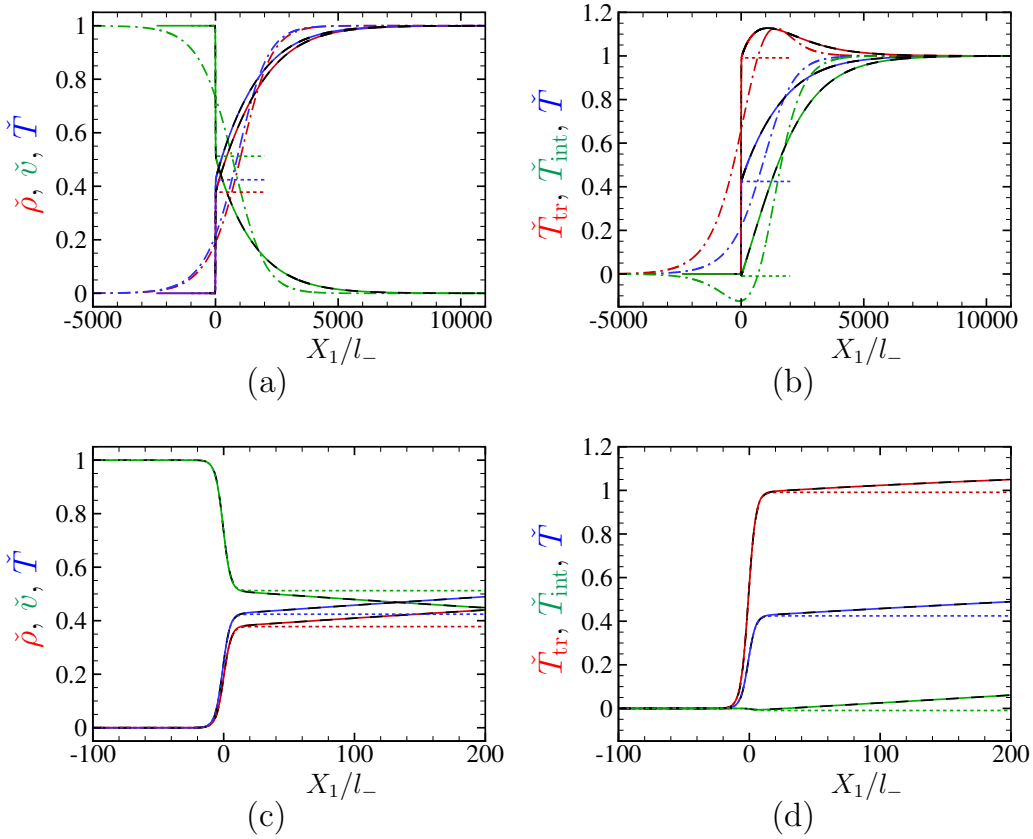

Figure 4. Profiles of $\check{\rho}$, $\check{v}$, $\check{T}$, $\check{T}_{\rm tr}$, and $\check{T}_{\rm int}$ in the case of the pseudo-CO_2 gas at $M_- = 1.3$ for $\mu_b/\mu = 1000$. (**a**,**c**) $\check{\rho}$, $\check{v}$, and $\check{T}$; (**b**,**d**) $\check{T}_{\rm tr}$, $\check{T}_{\rm int}$, and $\check{T}$. Panels (**c**,**d**) are, respectively, the magnified figures of panels (**a**,**b**) [except that the dot-dashed line is not included in panels (**c**,**d**)]. The solid line indicates the result based on the two-temperature NS equations (18), the dotted line that for $\theta = 0$ (or $\mu_b/\mu = \infty$) based on the same equations, and the dot-dashed line that based on the ordinary NS equations (14). The red, green, and blue lines indicate, respectively, $\check{\rho}$, $\check{v}$, and $\check{T}$ in panels (**a**,**c**) and $\check{T}_{\rm tr}$, $\check{T}_{\rm int}$, and $\check{T}$ in panels (**b**,**d**). The profiles based on the ES model (2) are shown by the black dashed line for all quantities.

Figures 5–7 show the profiles at $M_- = 3$ for $\mu_b/\mu = 10$ (Figure 5), 100 (Figure 6), and 1000 (Figure 7). As for the profiles at $M_- = 5$, only the result for $\mu_b/\mu = 1000$ is shown in Figure 8. The explanation of Figures 5–7 and that of Figure 8 are basically the same as the explanation of Figures 2–4 and that of Figure 4, respectively, so that they are omitted. It is noted that $T_+/T_- = 2.078$ and $\rho_+/\rho_- = 4.932$ at $M_- = 3$, and $T_+/T_- = 3.723$ and $\rho_+/\rho_- = 7.819$ at $M_- = 5$.

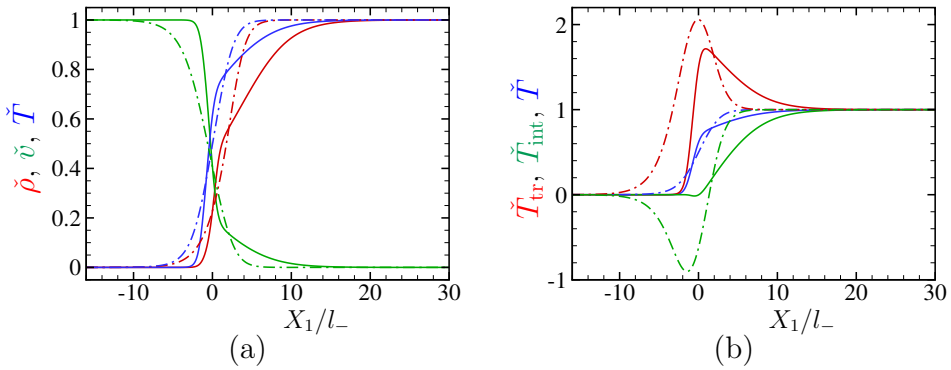

Figure 5. Profiles of $\check{\rho}$, $\check{v}$, $\check{T}$, $\check{T}_{\rm tr}$, and $\check{T}_{\rm int}$ in the case of the pseudo-CO_2 gas at $M_- = 3$ for $\mu_b/\mu = 10$. (**a**) $\check{\rho}$, $\check{v}$, and $\check{T}$; (**b**) $\check{T}_{\rm tr}$, $\check{T}_{\rm int}$, and $\check{T}$. See the caption of Figure 2.

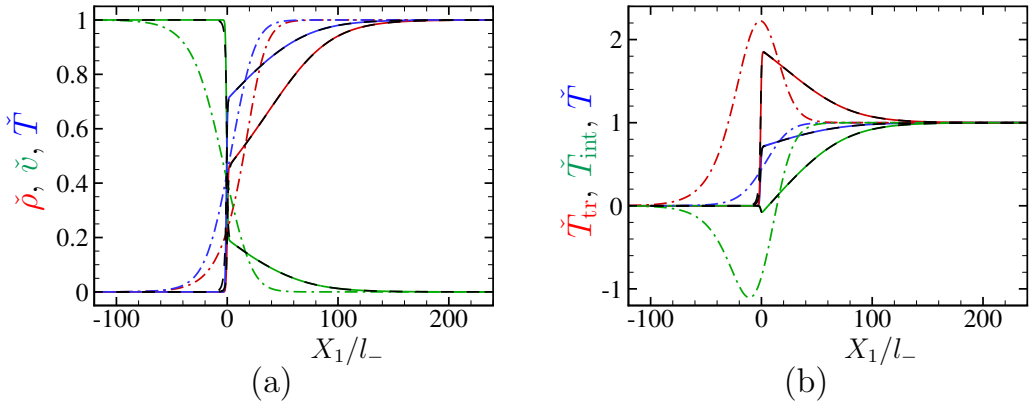

Figure 6. Profiles of $\check{\rho}$, $\check{v}$, $\check{T}$, $\check{T}_{\rm tr}$, and $\check{T}_{\rm int}$ in the case of the pseudo-CO_2 gas at $M_- = 3$ for $\mu_b/\mu = 100$. (**a**) $\check{\rho}$, $\check{v}$, and $\check{T}$; (**b**) $\check{T}_{\rm tr}$, $\check{T}_{\rm int}$, and $\check{T}$. See the caption of Figure 3.

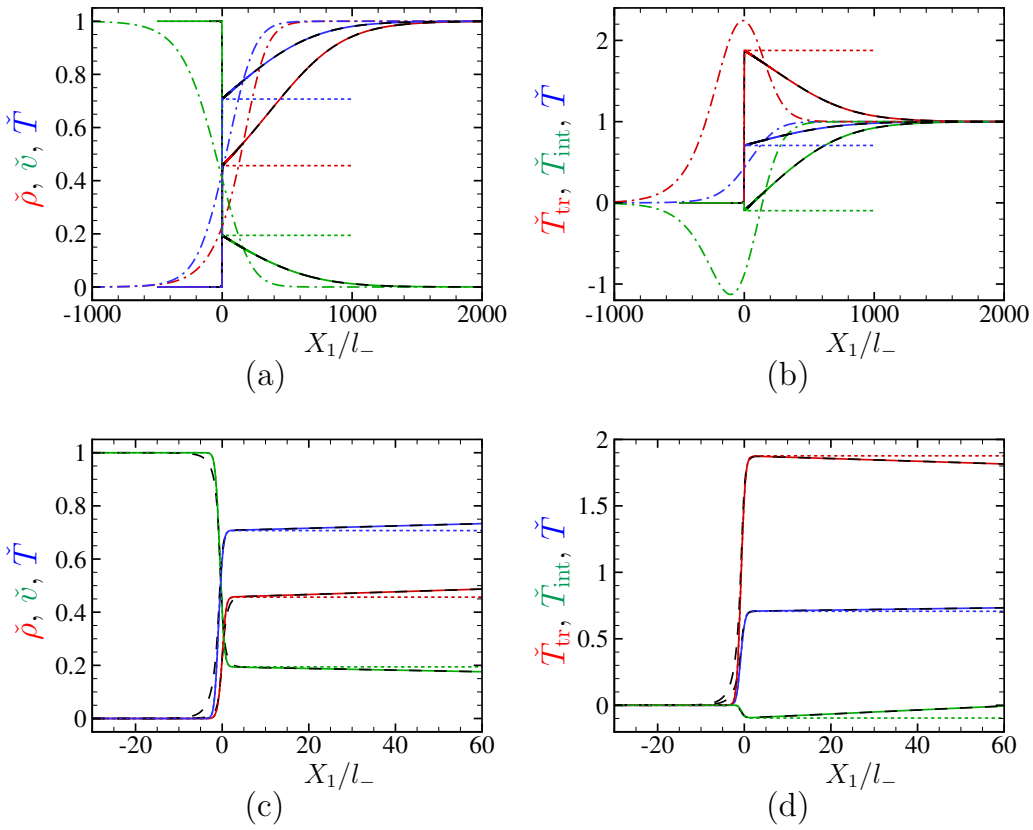

Figure 7. Profiles of $\check{\rho}$, $\check{v}$, $\check{T}$, $\check{T}_{\rm tr}$, and $\check{T}_{\rm int}$ in the case of the pseudo-CO_2 gas at $M_- = 3$ for $\mu_b/\mu = 1000$. (**a**,**c**) $\check{\rho}$, $\check{v}$, and $\check{T}$; (**b**,**d**) $\check{T}_{\rm tr}$, $\check{T}_{\rm int}$, and $\check{T}$. See the caption of Figure 4.

Figures 2–4 correspond to the case where the shock wave is rather weak ($M_- = 1.3$). Even for $\mu_b/\mu = 10$ (Figure 2), the profiles obtained by the two-temperature NS equations deviates significantly from those by the ordinary NS equations. For $\mu_b/\mu = 100$, the result based on the two-temperature NS equations, which agrees perfectly with that based on the ES model (2), shows separation of the profiles into the thin front layer with a steep change, which may be called a subshock, and the thick rear layer with a slow relaxation. This separation is not observed in the result based on the ordinary NS equations. When μ_b/μ increases up to 1000 (Figure 4), the separation becomes more prominent in the result based on the two-temperature NS equations as well as that based on the ES model (2), and the thickness of the shock wave is more than 5000 mean free paths. For a monatomic gas, it is known that the Navier–Stokes equations can describe the structure of weak shock waves relatively well. In contrast, for a polyatomic gas with large bulk viscosity, the ordinary NS

equations fail to describe the structure correctly even for weak shock waves. Contrarily, the two-temperature NS equations correctly describe the shock-wave structure for such a gas. As seen from Figures 4c,d, the subshock for large μ_b/μ coincides with the shock wave with $\theta = 0$ (or $\mu_b/\mu = \infty$).

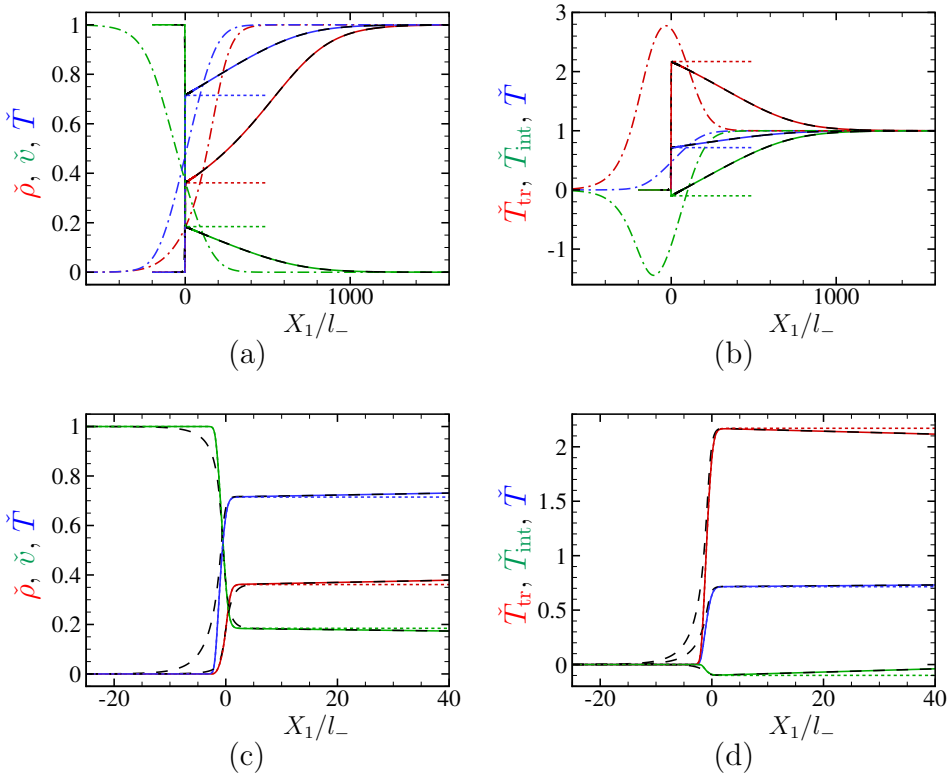

Figure 8. Profiles of $\check{\rho}$, $\check{v}$, $\check{T}$, $\check{T}_{\rm tr}$, and $\check{T}_{\rm int}$ in the case of the pseudo-CO_2 gas at $M_- = 5$ for $\mu_b/\mu = 1000$. (**a**,**c**) $\check{\rho}$, $\check{v}$, and $\check{T}$; (**b**,**d**) $\check{T}_{\rm tr}$, $\check{T}_{\rm int}$, and $\check{T}$. See the caption of Figure 4.

Figures 5–7 are for a higher upstream Mach number $M_- = 3$ and correspond to Figures 2–4, respectively. As in Figures 2–4, the profiles based on the two-temperature NS equations show the double-layer structure more eminently as μ_b/μ increases. However, the thickness of the rear layer for $\mu_b/\mu = 1000$, which is about 1000 mean free paths, is much smaller than that at $M_- = 1.3$ (cf. Figure 4). As seen from the magnified figures, Figure 7c,d, the two-temperature NS equations give a thinner and sharper subshock than the ES model (2) though the profiles based on both equations agree very well in the rear layer with slow relaxation. As Figure 8 shows, the deviation between the profiles based on the two-temperature NS equations and those based on the ES model in the subshock becomes larger for a relatively strong shock wave at $M_- = 5$, but their agreement in the thick rear layer is still very good. Figures 7c,d and 8c,d show that the profiles of the subshock for large μ_b/μ coincide with those of the shock wave with $\theta = 0$ (or $\mu_b/\mu = \infty$).

The double-layer structure of the shock profiles for CO_2 gas had long been known and was revisited using the macroscopic equations based on extended thermodynamics in [31,52,53], which motivated subsequent studies using kinetic theory [36,41,58]. The profiles with the double-layer structure was classified as type C in [31,52,53] (see also [41,58]). It should be mentioned that a similar double-layer structure is also observed for a shock wave in a ternary mixture of Euler gases with disparate masses [63].

We summarize the conclusion for the pseudo-CO_2 gas with large μ_b/μ obtained in the present computation as follows:

(i) The two-temperature NS equations are able to reproduce correct shock profiles for weak shock waves ($M_- = 1.3$).

(ii) For moderate and strong shock waves ($M_- = 3$ and 5), although the profiles obtained by the two-temperature NS equations deviate from those based on the ES model in the thin front layer (subshock), they agree very well in the thick rear layer. The two-temperature NS equations tend to give a thinner and sharper subshock.
(iii) The profiles of the subshock coincide with those of the shock wave with $\mu_b/\mu = \infty$.
(iv) The ordinary NS equations (with bulk viscosity) cannot be used to correctly describe the shock-wave structure even for weak shock waves ($M_- = 1.3$).

The properties (i)–(iii) have already been observed in cases where the specific heats are constant [36]. Therefore, focusing our attention on the property (iv), we investigate the shock-wave structure for other gases on the basis of the two-temperature and ordinary NS equations.

6.3.2. SF_6 Gas

For SF_6 gas, we set $T_- = 300\,\mathrm{K}$ and use the values of c_m ($m = 0, \ldots, 4$), $c_v(T_-)/R$, γ_-, and δ_- in Table 1 and those of s, Pr, and μ_b/μ in Table 2. Then, ν and θ are obtained as $\nu = -0.2412$ and $\theta = 2.224 \times 10^{-3}$ (note that these values are slightly different from those in Table 2). The pressure p_- or the density ρ_- at upstream infinity is not specified here. Once it is given, l_-, which appears in the figures as X_1/l_-, is determined using (12) (with $l_0 = l_-$, $T_0 = T_-$, and $\rho_0 = \rho_-$) and (29) [with $\mu(300\,\mathrm{K})$ in Table 2].

Figures 9–13 show the profiles of $\check{\rho}$, $\check{v}$, $\check{T}$, $\check{T}_{\mathrm{tr}}$, and $\check{T}_{\mathrm{int}}$ inside the shock wave at $M_- = 1.05$, $1.234\ldots$, 1.3, 3, and 5; in Figure 13, panels (c) and (d) are, respectively, the magnified figures of panels (a) and (b) (without the result based on the ordinary NS equations). The types and colors of the lines in the figures are the same as in Figure 2, so that the explanation is omitted. It is remarked that $(T_+/T_-,\ \rho_+/\rho_-) = (1.009,\ 1.098)$ ($M_- = 1.05$); $(1.039,\ 1.492)$ ($M_- = 1.234\ldots$); $(1.049,\ 1.643)$ ($M_- = 1.3$); $(1.368,\ 6.875)$ ($M_- = 3$); and $(1.938,\ 13.57)$ ($M_- = 5$).

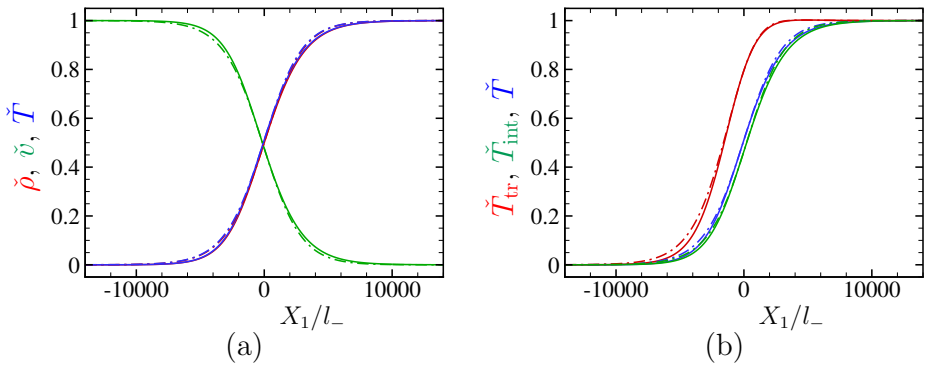

Figure 9. Profiles of $\check{\rho}$, $\check{v}$, $\check{T}$, $\check{T}_{\mathrm{tr}}$, and $\check{T}_{\mathrm{int}}$ in the case of SF_6 gas at $M_- = 1.05$. (**a**) $\check{\rho}$, $\check{v}$, and $\check{T}$; (**b**) $\check{T}_{\mathrm{tr}}$, $\check{T}_{\mathrm{int}}$, and $\check{T}$. See the caption of Figure 2.

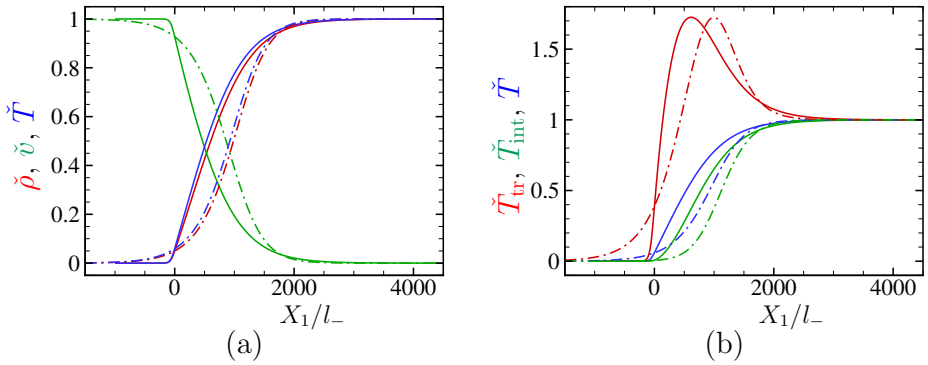

Figure 10. Profiles of $\check{\rho}$, $\check{v}$, $\check{T}$, $\check{T}_{\mathrm{tr}}$, and $\check{T}_{\mathrm{int}}$ in the case of SF_6 gas at $M_- = 1.234\ldots$. (**a**) $\check{\rho}$, $\check{v}$, and $\check{T}$; (**b**) $\check{T}_{\mathrm{tr}}$, $\check{T}_{\mathrm{int}}$, and $\check{T}$. See the caption of Figure 2.

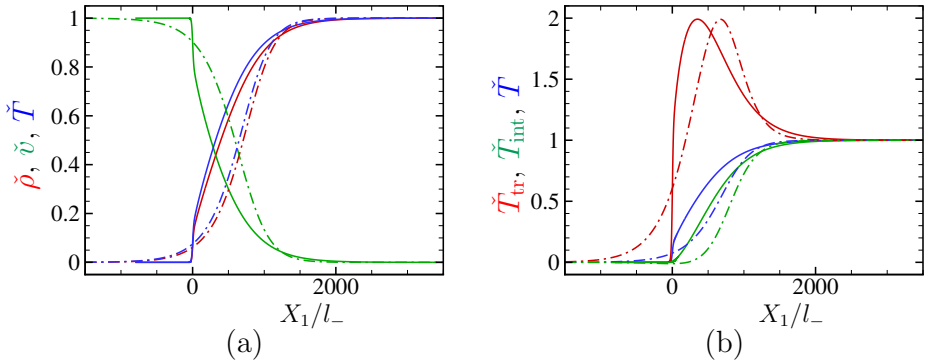

Figure 11. Profiles of $\check{\rho}$, $\check{v}$, $\check{T}$, $\check{T}_{\rm tr}$, and $\check{T}_{\rm int}$ in the case of SF_6 gas at $M_- = 1.3$. (**a**) $\check{\rho}$, $\check{v}$, and $\check{T}$; (**b**) $\check{T}_{\rm tr}$, $\check{T}_{\rm int}$, and $\check{T}$. See the caption of Figure 2.

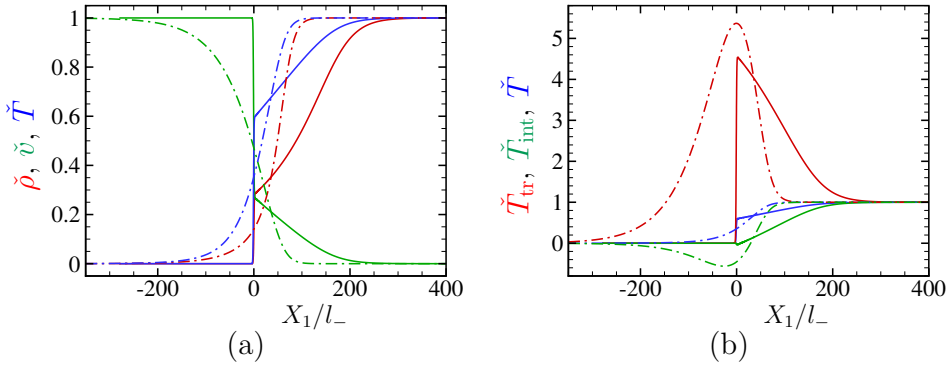

Figure 12. Profiles of $\check{\rho}$, $\check{v}$, $\check{T}$, $\check{T}_{\rm tr}$, and $\check{T}_{\rm int}$ in the case of SF_6 gas at $M_- = 3$. (**a**) $\check{\rho}$, $\check{v}$, and $\check{T}$; (**b**) $\check{T}_{\rm tr}$, $\check{T}_{\rm int}$, and $\check{T}$. See the caption of Figure 2.

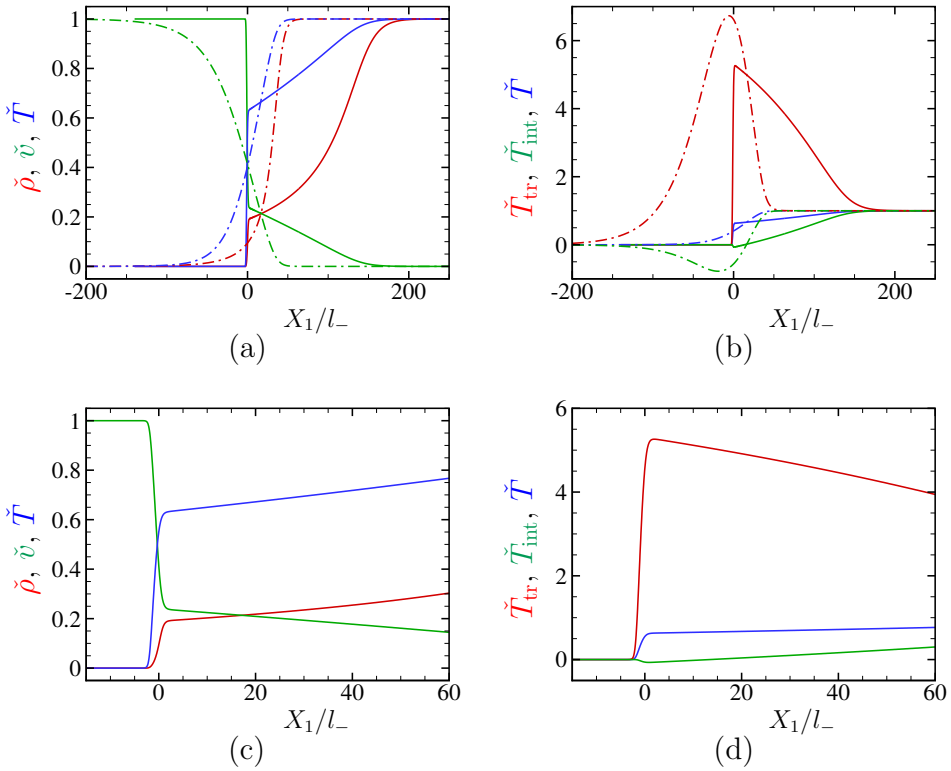

Figure 13. Profiles of $\check{\rho}$, $\check{v}$, $\check{T}$, $\check{T}_{\rm tr}$, and $\check{T}_{\rm int}$ in the case of SF_6 gas at $M_- = 5$. (**a**,**c**) $\check{\rho}$, $\check{v}$, and $\check{T}$; (**b**,**d**) $\check{T}_{\rm tr}$, $\check{T}_{\rm int}$, and $\check{T}$. Panels (**c**,**d**) are, respectively, the magnified figures of panels (**a**,**b**). See the caption of Figure 2.

When $M_- = 1.05$ (Figure 9), which corresponds to a very weak shock, the profiles are smooth, and the profiles based on the ordinary NS equations (14) do not differ much from those based on the two-temperature NS equations (18). These smooth profiles are classified as type A in [31,52,53] (see also [41,58]). However, when $M_- = 1.234\ldots$ (Figure 10), the profiles start suddenly except for $\check{T}_{\rm int}$ and are quite different from those in Figure 9 though M_- has been increased slightly. These profiles with a sudden start are classified as type B in [31,52,53] (see also [41,58]). Although the shock wave is still weak, the ordinary NS equations cannot describe the sudden start of the profiles. The value $M_- = 1.234\ldots$ corresponds to the sonic point $\widetilde{M}_- = 1$ of a different upstream Mach number $\widetilde{M}_- = v_-/\sqrt{5RT_-/3}$, that is, the upstream Mach number when the gas is regarded as a monatomic gas, or when the internal modes are frozen (see [58]). At $M_- = 1.3$ (Figure 11), one can observe the appearance of a thin front layer with a steep change (subshock). As in the case of pseudo-CO_2 gas (see Figure 4), the ordinary NS equations cannot describe the profiles with a subshock. As M_- is increased to 3 (Figure 12) and further to 5 (Figure 13), the amplitude of the subshock increases, and the change of physical quantities becomes steeper there. We recall that in the case of the pseudo-CO_2 gas (Figures 7 and 8), the subshock based on the two-temperature NS equations (18) is much thinner than that based on the original ES model (2) for moderately strong shock waves. Therefore, we cannot expect that the profiles inside the subshock in Figures 13c,d are accurate. Nevertheless, the jump over the subshock and the profiles in the thick rear layer are expected to be correct in Figure 13. With the exception of Figure 9 corresponding to the profiles of type A, the ordinary NS equations (with the bulk viscosity) provide completely incorrect profiles.

6.3.3. CH_4 Gas

Finally, we present some results for CH_4 gas. We also set $T_- = 300\,\mathrm{K}$ here and use the values of c_m ($m = 0, \ldots, 4$), $c_{\rm v}(T_-)/R$, γ_-, and δ_- in Table 1 and those of s, Pr, and μ_b/μ in Table 2. Then, ν and θ are obtained as $\nu = -0.3112$ and $\theta = 1.997 \times 10^{-3}$ (note that these values are slightly different from those in Table 2). The pressure p_- or the density ρ_- at upstream infinity is not specified here (see the first paragraph in Section 6.3.2). Figures 14–18 show the profiles of $\check{\rho}$, $\check{v}$, $\check{T}$, $\check{T}_{\rm tr}$, and $\check{T}_{\rm int}$ inside the shock wave at $M_- = 1.05$, $1.131\ldots$, 1.3, 3, and 5; in Figure 18, panels (c) and (d) are, respectively, the magnified figures of panels (a) and (b) (without the result based on the ordinary NS equations). The different types and colors of the lines in the figures are the same as in Figure 2, thus the explanation is omitted. We remark that $(T_+/T_-,\ \rho_+/\rho_-) = (1.026,\ 1.089)$ ($M_- = 1.05$); $(1.067,\ 1.240)$ ($M_- = 1.131\ldots$); $(1.147,\ 1.563)$ ($M_- = 1.3$); $(2.060,\ 5.042)$ ($M_- = 3$); and $(3.408,\ 8.747)$ ($M_- = 5$).

The value $M_- = 1.131\ldots$ in Figure 15 corresponds to $\widetilde{M}_- = 1$, as in Figure 10. Although the local values of the profile are different from those for SF_6 gas shown in Figures 9–13, the qualitative behavior at respective values of M_- is similar to SF_6 gas, and we therefore do not repeat similar explanations here.

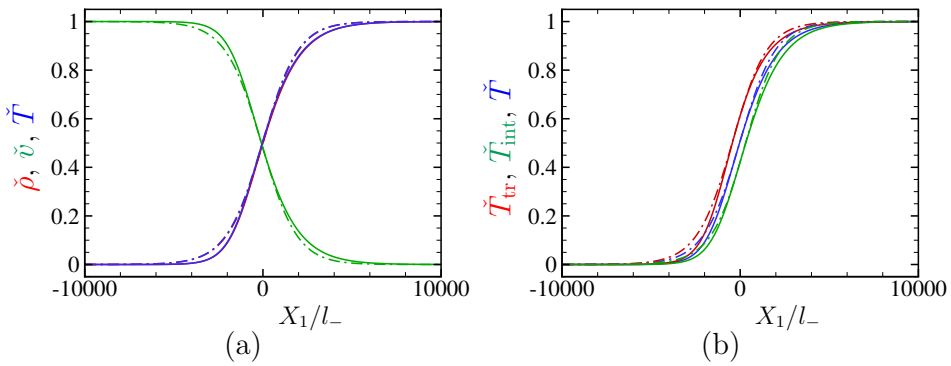

Figure 14. Profiles of $\check{\rho}$, $\check{v}$, $\check{T}$, $\check{T}_{\rm tr}$, and $\check{T}_{\rm int}$ in the case of CH_4 gas at $M_- = 1.05$. (**a**) $\check{\rho}$, $\check{v}$, and $\check{T}$; (**b**) $\check{T}_{\rm tr}$, $\check{T}_{\rm int}$, and $\check{T}$. See the caption of Figure 2.

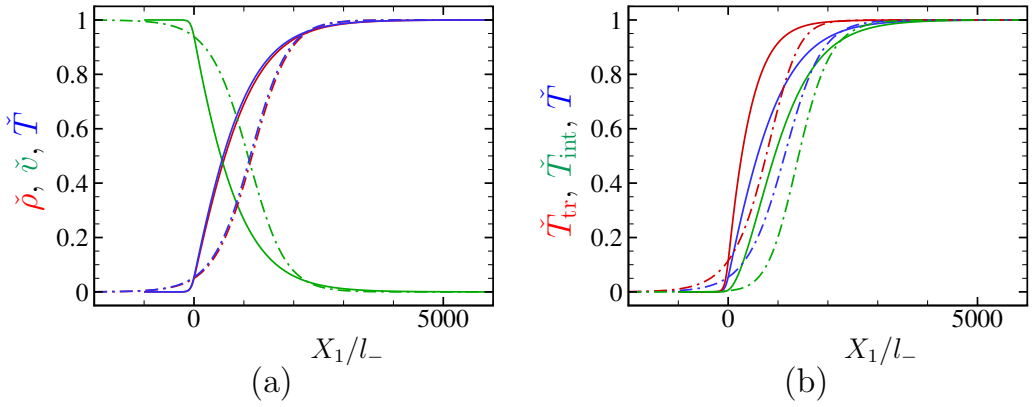

Figure 15. Profiles of $\check{\rho}$, $\check{v}$, $\check{T}$, $\check{T}_{\rm tr}$, and $\check{T}_{\rm int}$ in the case of CH_4 gas at $M_- = 1.131\ldots$. (**a**) $\check{\rho}$, $\check{v}$, and $\check{T}$; (**b**) $\check{T}_{\rm tr}$, $\check{T}_{\rm int}$, and $\check{T}$. See the caption of Figure 2.

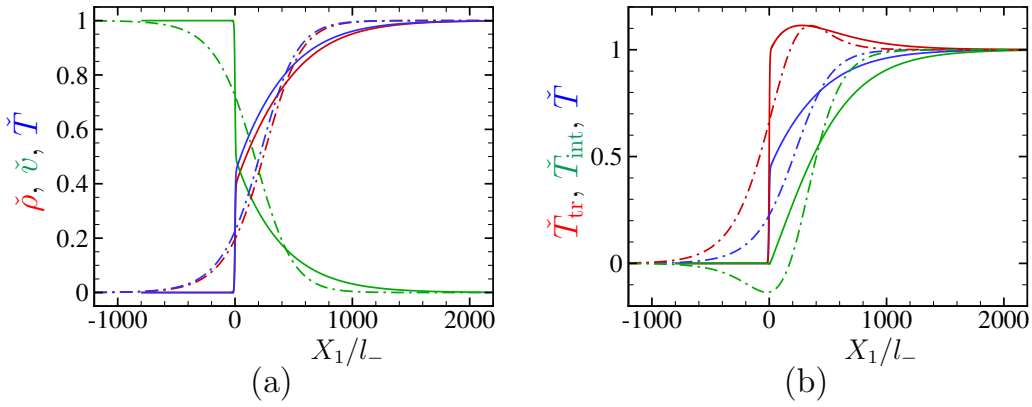

Figure 16. Profiles of $\check{\rho}$, $\check{v}$, $\check{T}$, $\check{T}_{\rm tr}$, and $\check{T}_{\rm int}$ in the case of CH_4 gas at $M_- = 1.3$. (**a**) $\check{\rho}$, $\check{v}$, and $\check{T}$; (**b**) $\check{T}_{\rm tr}$, $\check{T}_{\rm int}$, and $\check{T}$. See the caption of Figure 2.

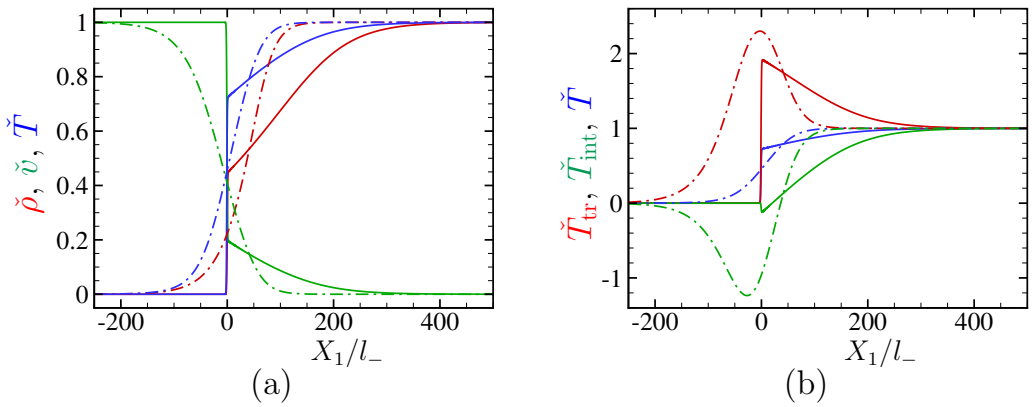

Figure 17. Profiles of $\check{\rho}$, $\check{v}$, $\check{T}$, $\check{T}_{\rm tr}$, and $\check{T}_{\rm int}$ in the case of CH_4 gas at $M_- = 3$. (**a**) $\check{\rho}$, $\check{v}$, and $\check{T}$; (**b**) $\check{T}_{\rm tr}$, $\check{T}_{\rm int}$, and $\check{T}$. See the caption of Figure 2.

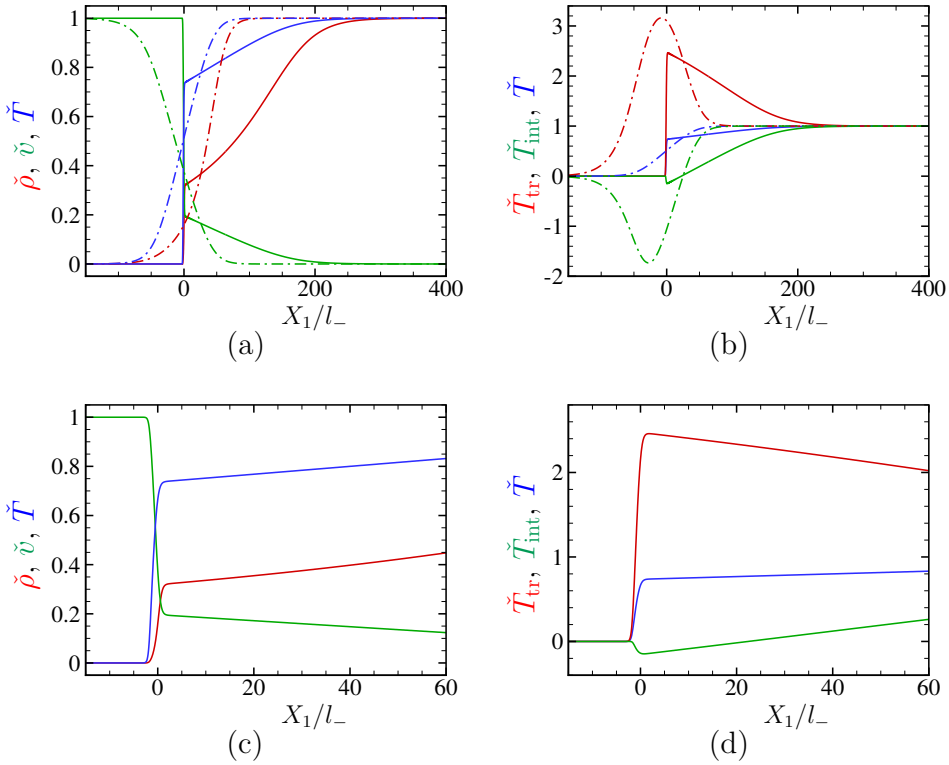

Figure 18. Profiles of $\check{\rho}$, $\check{v}$, $\check{T}$, $\check{T}_{\rm tr}$, and $\check{T}_{\rm int}$ in the case of CH_4 gas at $M_- = 5$. (**a**,**c**) $\check{\rho}$, $\check{v}$, and $\check{T}$; (**b**,**d**) $\check{T}_{\rm tr}$, $\check{T}_{\rm int}$, and $\check{T}$. Panels (**c**,**d**) are, respectively, the magnified figures of panels (**a**,**b**). See the caption of Figure 2.

7. Concluding Remarks

In our recent paper [36], we derived two-temperature Navier–Stokes equations for a polyatomic gas with slow relaxation of the internal modes from the ES model [21,22]. In this model, slow relaxation of the internal modes is equivalent to large values of the ratio of bulk viscosity to viscosity μ_b/μ. The resulting Navier–Stokes equations were then successfully applied to the numerical analysis of the shock-structure problem. All these results pertain to a gas with constant specific heats (calorically perfect gas).

In the present paper, we have extended the two-temperature Navier–Stokes equations to a polyatomic gas whose specific heats are not constant but depend on temperature (thermally perfect gas) using the ES model for such a gas proposed in [41]. Then, using the extended two-temperature Navier–Stokes equations, we numerically analyzed the structure of a plane shock wave for certain gases bearing large values of μ_b/μ, i.e., CO_2, SF_6, and CH_4. The same problem has also been analyzed by using the ordinary Navier–Stokes equations with a single temperature and bulk viscosity derived from the same extended ES model.

We first confirmed for CO_2 gas (more precisely, pseudo-CO_2 gas) that, as in the case of a calorically perfect gas [36], the two-temperature Navier–Stokes equations recover the shock profiles obtained by the numerical analysis of the ES model very well for weak shock waves and sufficiently well even for moderately strong shock waves. Subsequently, we showed that the shock profiles obtained by the ordinary Navier–Stokes equations differ significantly from those based on the two-temperature Navier–Stokes equations even for weak shock waves. Notably, the double-layer structure with a thin front layer (subshock) and a thick rear layer, as obtained by the two-temperature Navier–Stokes equations, cannot be described by the ordinary Navier–Stokes equations even qualitatively. This drawback of the ordinary Navier–Stokes equations was also demonstrated for SF_6 and CH_4 gases.

Therefore, we may conclude that the ordinary Navier–Stokes equations with bulk viscosity are inappropriate for polyatomic gases with large values of μ_b/μ, even at the so-

called Navier–Stokes level. For such gases, one should use more appropriate macroscopic equations, such as the two-temperature Navier–Stokes equations derived in this paper.

The present two-temperature Navier–Stokes equations are derived from the ES model (2) with a single energy variable $\mathcal{E}$ for all the internal modes. Therefore, if, for instance, one of the vibrational modes relaxes slowly, we suppose that the *internal modes* relax slowly and that the two-temperature Navier–Stokes equations are applicable. In this sense, the latter equations are rather primitive. Recently, more sophisticated ES models using two separate energy variables for rotational and vibrational modes have been proposed [26,27]. With the help of these new models and of an appropriate parameter setting, one may derive multi-temperature Navier–Stokes equations with the translational, rotational, and vibrational temperatures. The derivation of such equations would be an interesting and important subject as the next step.

Author Contributions: Conceptualization, S.K. and K.A.; methodology, S.K. and K.A.; formal analysis, S.K. and K.A; numerical analysis, S.K.; writing—original draft preparation, K.A.; writing—review and editing, S.K.; All authors have read and agreed to the published version of the manuscript.

Funding: This research received no external funding.

Institutional Review Board Statement: Not applicable.

Informed Consent Statement: Not applicable.

Data Availability Statement: Not applicable.

Conflicts of Interest: The authors declare no conflict of interest.

References

1. Anderson, J.D., Jr. *Hypersonic and High Temperature Gas Dynamics*; McGraw-Hill: New York, NY, USA, 1989.
2. Park, C. *Nonequilibrium Hypersonic Aerothermodynamics*; John Wiley & Sons: New York, NY, USA, 1990.
3. Nagnibeda, E.; Kustova, E. *Non-Equilibrium Reacting Gas Flows: Kinetic Theory of Transport and Relaxation Processes*; Springer: Berlin, Germany, 2009.
4. Boyd, I.D.; Schwartzentruber, T.E. *Nonequilibrium Gas Dynamics and Molecular Simulation*; Cambridge University Press: Cambridge, UK, 2017.
5. Wang Chang, C.S.; Uhlenbeck, G.E. *Transport Phenomena in Polyatomic Gases*; Engineering Research Institute Report CM-681; University of Michigan: Ann Arbor, MI, USA, 1951.
6. Ferziger, J.H.; Kaper, H.G. *Mathematical Theory of Transport Processes in Gases*; North Holland: Amsterdam, The Netherlands, 1972.
7. McCourt, F.R.W.; Beenakker, J.J.M.; Köhler, W.E.; Kuščer, I. *Nonequilibrium Phenomena in Polyatomic Gases, Volume 1: Dilute Gases*; Clarendon: Oxford, UK, 1990.
8. Giovangigli, V. *Multicomponent Flow Modeling*; Birkhäuser: Boston, MA, USA, 1999.
9. Borgnakke, C.; Larsen, P.S. Statistical collision model for Monte Carlo simulation of polyatomic gas mixture. *J. Comp. Phys.* **1975**, *18*, 405–420. [CrossRef]
10. Bourgat, J.-F.; Desvillettes, L.; Le Tallec, P.; Perthame, B. Microreversible collisions for polyatomic gases and Boltzmann's theorem. *Eur. J. Mech. B Fluids* **1994**, *13*, 237–254.
11. Desvillettes, L.; Monaco, R.; Salvarani, F. A kinetic model allowing to obtain the energy law of polytropic gases in the presence of chemical reactions. *Eur. J. Mech. B Fluids* **2005**, *24*, 219–236. [CrossRef]
12. Borsoni, T.; Bisi, M.; Groppi, M. A general framework for the kinetic modelling of polyatomic gases. *Commun. Math. Phys.* **2022**, *393*, 215–266. [CrossRef]
13. Pavić-Čolić, M.; Simić, S. Kinetic description of polyatomic gases with temperature-dependent specific heats. *Phys. Rev. Fluids* **2022**, *7*, 083401. [CrossRef]
14. Boudin, L.; Rossi, A.; Salvarani, F. A kinetic model of polyatomic gas with resonant collisions. *Ricerche Mat.* **2022**. [CrossRef]
15. Gamba, I.M.; Pavić-Čolić, M. On the Cauchy problem for Boltzmann equation modelling a polyatomic gas. *arXiv Prepr.* **2020**, arXiv:2005.01017.
16. Brull, S.; Shahine, M.; Thieullen, P. Compactness property of the linearized Boltzmann operator for a diatomic single gas model. *Netw. Heterog. Media* **2022**, *17*, 847–861. [CrossRef]
17. Bernhoff, N. Linearized Boltzmann collision operator: II. Polyatomic molecules modeled by a continuous internal energy variable. *arXiv Prepr.* **2022**, arXiv:2201.01377.
18. Morse, T.F. Kinetic model for gases with internal degrees of freedom. *Phys. Fluids* **1964**, *7*, 159–169. [CrossRef]
19. Holway Jr., L.H. New statistical models for kinetic theory: Methods of construction. *Phys. Fluids* **1966**, *9*, 1658–1673. [CrossRef]
20. Rykov, V.A. A model kinetic equation for a gas with rotational degrees of freedom. *Fluid Dyn.* **1975**, *10*, 959–966. [CrossRef]

21. Andries, P.; Le Tallec, P.; Perlat, J.-P.; Perthame, B. The Gaussian-BGK model of Boltzmann equation with small Prandtl number. *Eur. J. Mech. B Fluids* **2000**, *19*, 813–830. [CrossRef]
22. Brull, S.; Schneider, J. On the ellipsoidal statistical model for polyatomic gases. *Contin. Mech. Thermodyn.* **2009**, *20*, 489–508. [CrossRef]
23. Rahimi, B.; Struchtrup, H. Capturing non-equilibrium phenomena in rarefied polyatomic gases: A high-order macroscopic model. *Phys. Fluids* **2014**, *26*, 052001. [CrossRef]
24. Bisi, M.; Spiga, G. On kinetic models for polyatomic gases and their hydrodynamic limits. *Ric. Mat.* **2017**, *66*, 113–124. [CrossRef]
25. Baranger, C.; Dauvois, Y.; Marois, G.; Mathé, J.; Mathiaud, J.; Mieussens, L. A BGK model for high temperature rarefied gas flows. *Eur. J. Mech. B Fluids* **2020**, *80*, 1–12. [CrossRef]
26. Dauvois, Y.; Mathiaud, J.; Mieussens, L. An ES-BGK model for polyatomic gases in rotational and vibrational nonequilibrium. *Eur. J. Mech. B Fluids* **2021**, *88*, 1–16. [CrossRef]
27. Mathiaud, J.; Mieussens, L.; Pfeiffer, M. An ES-BGK model for diatomic gases with correct relaxation rates for internal energies. *Eur. J. Mech. B Fluids* **2022**, *96*, 65–77. [CrossRef]
28. Myong, R.S. Coupled nonlinear constitutive models for rarefied and microscale gas flows: Subtle interplay of kinematics and dissipation effects. *Contin. Mech. Thermodyn.* **2009**, *21*, 389–399. [CrossRef]
29. Arima, T.; Taniguchi, S.; Ruggeri, T.; Sugiyama, M. Extended thermodynamics of real gases with dynamic pressure: An extension of Meixner's theory. *Phys. Lett. A* **2012**, *376*, 2799–2803. [CrossRef]
30. Pavić, M.; Ruggeri, T.; Simić, S. Maximum entropy principle for rarefied polyatomic gases. *Phys. A* **2013**, *392*, 1302–1317. [CrossRef]
31. Taniguchi, S.; Arima, T.; Ruggeri, T.; Sugiyama, M. Overshoot of the non-equilibrium temperature in the shock wave structure of a rarefied polyatomic gas subject to the dynamic pressure. *Int. J. Non-Linear Mech.* **2016**, *79*, 66–75. [CrossRef]
32. Arima, T.; Ruggeri, T.; Sugiyama, M. Rational extended thermodynamics of a rarefied polyatomic gas with molecular relaxation processes. *Phys. Rev. E* **2017**, *96*, 042143. [CrossRef]
33. Pavić-Čolić, M.; Madjarević, D.; Simić, S. Polyatomic gases with dynamic pressure: Kinetic non-linear closure and the shock structure. *Int. J. Non-Linear Mech.* **2017**, *92*, 160–175. [CrossRef]
34. Bisi, M.; Ruggeri, T.; Spiga, G. Dynamical pressure in a polyatomic gas: Interplay between kinetic theory and extended thermodynamics. *Kin. Rel. Models* **2018**, *11*, 71–95. [CrossRef]
35. Ruggeri, T.; Sugiyama, M. *Classical and Relativistic Rational Extended Thermodynamics of Gases*; Springer: Cham, Switzerland, 2021.
36. Aoki, K.; Bisi, M.; Groppi, M.; Kosuge, S. Two-temperature Navier–Stokes equations for a polyatomic gas derived from kinetic theory. *Phys. Rev. E* **2020**, *102*, 023104. [CrossRef]
37. Chapman, S.; Cowling, T.G. *The Mathematical Theory of Non-Uniform Gases*, 3rd ed.; Cambridge University Press: Cambridge, UK, 1991.
38. Grad, H. Principles of the kinetic theory of gases. In *Handbuch der Physik*; Band XII; Flügge, S., Ed.; Springer: Berlin, Germany, 1958; pp. 205–294.
39. Cercignani, C. *The Boltzmann Equation and Its Applications*; Springer: Berlin, Germany, 1988.
40. Sone, Y. *Molecular Gas Dynamics: Theory, Techniques, and Applications*; Birkhäuser: Boston, MA, USA, 2007; Supplementary Notes and Errata. Available online: http://hdl.handle.net/2433/66098 (accessed on 21 July 2019).
41. Kosuge, S.; Kuo, H.-W.; Aoki, K. A kinetic model for a polyatomic gas with temperature-dependent specific heats and its application to shock-wave structure. *J. Stat. Phys.* **2019**, *177*, 209–251. [CrossRef]
42. Park, C.; Yoon, S. Calculation of real-gas effects on blunt-body trim angles. *AIAA J.* **1992**, *30*, 999–1007. [CrossRef]
43. Park, C.; Lee, S.-H. Validation of multitemperature nozzle flow code. *J. Thermophys. Heat Trans.* **1995**, *9*, 9–16. [CrossRef]
44. Bruno, D.; Giovangigli, V. Relaxation of internal temperature and volume viscosity. *Phys. Fluids* **2011**, *23*, 093104; Erratum in *Phys. Fluids* **2013**, *25*, 039902. [CrossRef]
45. Bruno, D.; Giovangigli, V. Internal energy relaxation processes and bulk viscosities in fluids. *Fluids* **2022**, *7*, 356. [CrossRef]
46. Kosuge, S.; Aoki, K.; Bisi, M.; Groppi, M.; Martalò, G. Boundary conditions for two-temperature Navier–Stokes equations for a polyatomic gas. *Phys. Rev. Fluids* **2021**, *6*, 083401. [CrossRef]
47. Bird, G.A. *Molecular Gas Dynamics and the Direct Simulation of Gas Flows*; Oxford University Press: Oxford, UK, 1994.
48. Smiley, E.F.; Winkler, E.H.; Slawsky, Z.I. Measurement of the vibrational relaxation effect in CO_2 by means of shock tube interferograms. *J. Chem. Phys.* **1952**, *20*, 923–924. [CrossRef]
49. Smiley, E.F.; Winkler, E.H. Shock-tube measurements of vibrational relaxation. *J. Chem. Phys.* **1954**, *22*, 2018–2022. [CrossRef]
50. Griffith, W.D.; Kenny, A. On fully-dispersed shock waves in carbon dioxide. *J. Fluid Mech.* **1957**, *3*, 286–289. [CrossRef]
51. Johannesen, N.H.; Zienkiewicz, H.K.; Blythe, P.A.; Gerrard, J.H. Experimental and theoretical analysis of vibrational relaxation regions in carbon dioxide. *J. Fluid Mech.* **1962**, *13*, 213–225. [CrossRef]
52. Taniguchi, S.; Arima, T.; Ruggeri, T.; Sugiyama, M. Effect of the dynamic pressure on the shock wave structure in a rarefied polyatomic gas. *Phys. Fluids* **2014**, *26*, 016103. [CrossRef]
53. Taniguchi, S.; Arima, T.; Ruggeri, T.; Sugiyama, M. Thermodynamic theory of the shock wave structure in a rarefied polyatomic gas: Beyond the Bethe-Teller theory. *Phys. Rev. E* **2014**, *89*, 013025. [CrossRef]

54. Alekseev, I.V.; Kosareva, A.A.; Kustova, E.V.; Nagnibeda, E.A. Various continuum approaches for studying shock wave structure in carbon dioxide. In Proceedings of the The Eighth Polyakhov's Reading: Proceedings of the International Scientific Conference on Mechanics, Saint Petersburg, Russia, 29 January–2 February 2018; Kustova, E., Leonov, G., Morosov, N., Yushkov, M., Mekhonoshina, M. Eds.; AIP: Melville, NY, USA, 2018; p. 060001.
55. Alekseev, I.V.; Kosareva, A.A.; Kustova, E.V.; Nagnibeda, E.A. Shock waves in carbon dioxide: Simulations using different kinetic-theory models. In Proceedings of the 31st International Symposium on Rarefied Gas Dynamics, Glasgow, UK, 23–27 July 2018; Zhang, Y., Emerson, D.R., Lockerby, D., Wu, L. Eds.; AIP: Melville, NY, USA, 2019; p. 060005.
56. Kustova, E.; Mekhonoshina, M.; Kosareva, A. Relaxation processes in carbon dioxide. *Phys. Fluids* **2019**, *31*, 046104. [CrossRef]
57. Alekseev, I.; Kustova, E. Extended continuum models for shock waves in CO_2. *Phys. Fluids* **2021**, *33*, 096101. [CrossRef]
58. Kosuge, S.; Aoki, K. Shock-wave structure for a polyatomic gas with large bulk viscosity. *Phys. Rev. Fluids* **2018**, *3*, 023401. [CrossRef]
59. Japan Society of Thermophysical Properties (Ed.) *Thermophysical Properties Handbook*; Yokendo: Tokyo, Japan, 1990. (In Japanese)
60. Uribe, F.J.; Mason, E.A.; Kestin, J. Thermal conductivity of nine polyatomic gases at low density. *J. Phys. Chem. Ref. Data* **1990**, *19*, 1123–1136. [CrossRef]
61. Cramer, M.S. Numerical estimates for the bulk viscosity of ideal gases. *Phys. Fluids* **2012**, *24*, 066102. [CrossRef]
62. Boushehri, A.; Bzowski, J.; Kestin, J.; Mason, E.A. Equilibrium and transport properties of eleven polyatomic gases at low density. *J. Phys. Chem. Ref. Data* **1987**, *16*, 445–466; Erratum in *J. Phys. Chem. Ref. Data* **1988**, *17*, 255. [CrossRef]
63. Madjarević, D.; Pavić-Čolić, M.; Simić, S. Shock structure and relaxation in the multi-component mixture of Euler fluids. *Symmetry* **2021**, *13*, 955. [CrossRef]